34

FRAGMENTING THE UNIVERSE . 4 .

IV. THE CLUSTERING PROPERTIES OF VORONOI FOAMS

Rien van de Weygaert[1,2]

[1] CITA, 60 St. George St.,Toronto, Ontario, Canada
[2] Sterrewacht Leiden, Leiden, The Netherlands

ABSTRACT

The use of the Voronoi foam in a cosmological context is treated, with particular emphasis on their clustering properties. Firstly, the phenomological background of the introduction of the Voronoi foam as a description of the large scale distribution of galaxies is discussed. This is followed by a treatment of the clustering properties of Voronoi vertices, which are identified as the clusters in a Voronoi foam. A remarkable property is that the vertex-vertex correlation function has a slope and amplitude which is very close to the cluster-cluster correlation function extracted from the observations. Finally, an analysis is presented of the clustering properties of particles distributed within a Voronoi foam, both in the walls and in the filaments, as well as of combined distributions.

Subject headings: Cosmology : theory – Galaxies: clustering – large-scale structure of the Universe

1. Introduction

The Voronoi foam is a unique, simple and tractable statistical model for a distribution of galaxies that is confined to sheets, filaments, and clusters surrounding voids. The principal significance of the Voronoi tessellation in a cosmological context is that it is a very useful mathematical model from which we can learn several general properties of clustering in cellular structures. In addition, it may give a reasonably accurate *quantitative* description of some specific physical models of structure formation, in particular models wherein voids, or bubbles, play a dominant dynamical role (see e.g. Dubinski *et al.* 1993). Models to which the Voronoi foams apply can be either gravitational instability models (Icke & Van de Weygaert 1987; Van de Weygaert & Icke 1989), although its success in that case will depend on the spectrum and type of primordial fluctuations, and models in which the driving force is due to explosions (Ikeuchi 1981; Ostriker & Cowie 1981; Yoshioka & Ikeuchi 1989; Thompson, Weinberg & Juskiewicz 1989), assuming the explosions took place around the same epoch and were equally powerful. If we assume the galaxies populate the walls and edges of the Voronoi cells, the Voronoi model qualitatively reproduces the observed pattern of cells, sheets and filaments in the observed galaxy distribution. Although the model cannot say much about the pattern of the galaxy distribution on smaller scales, within the sheets, it can be considered as a useful prescription for the spatial distribution of the sheets themselves.

Formally a Voronoi tessellation can be defined as follows. Assume that we have a distribution of a countable set Φ of nuclei $\{x_i\}$ in $\Re^d$. Let $\vec{x}_1, \vec{x}_2, \vec{x}_3, \ldots$ be the coordinates of the nuclei. Then, the *Voronoi region* Π_i of nucleus i is defined by the following set of points $\vec{x}$ of the space:

$$\Pi_i = \{\vec{x} | d(\vec{x}, \vec{x}_i) < d(\vec{x}, \vec{x}_j) \qquad \text{for all } j \neq i\}, \tag{1}$$

where $d(\vec{x}, \vec{y})$ is the Euclidian distance between $\vec{x}$ and $\vec{y}$. In other words, Π_i is the set of points which is nearer to $\vec{x}_i$ than to $\vec{x}_j$, $\quad j \neq i$. Note that each region Π_i is the intersection of the open half-spaces bounded by the perpendicular bisectors of the segments joining $\vec{x}_i$ with each of the other

$\vec{x}_j$'s. Hence, Voronoi regions are convex polyhedra (3-D) with finite size according to definition (1). Each Π_i is called a *Voronoi polyhedron*. The complete set of $\{\Pi_i\}$ constitute a tessellation of $\Re^d$, the *Voronoi tessellation* $\mathcal{V}(\Phi)$ relative to Φ. In two-dimensional space some authors refer to it as the Dirichlet or Thiessen tessellation. Known formulae for $\mathcal{V}(\Phi)$ are almost entirely confined to the case when Φ is a stationary Poisson process.

Voronoi tessellations are used in many fields of applied science, such as molecular physics, geology, and metallurgy. They are one of the main objects of study in the field of stochastic geometry, which is the branch of mathematics that is involved with the problems which arise when probability distributions are ascribed to geometric objects or operations. Amongst others, it provides us with the mathematical background for studying point patterns, such as the distribution of galaxies. A subbranch, stereology, is involved with the study of the relation between three-dimensional geometric patterns and lower-dimensional sections through them. The applications of stereology to the interpretation of the results of the "slice" and "pencil-beam" galaxy redshift surveys are obvious.

Kiang (1966) was the first to apply Voronoi tessellations to astrophysics, in his study of the mass spectrum obtained in the fragmentation of interstellar clouds. Matsuda & Shima (1984) were the first to propose the use of Voronoi tessellations in cosmology. They pointed out the similarity between two-dimensional Voronoi tessellations and the outcome of numerical clustering simulations in a neutrino-dominated universe by Melott (1983). Independently, Voronoi tessellations were introduced into cosmology by Icke & Van de Weygaert (1987). In their paper (IW) they studied the statistical properties of two-dimensional Voronoi tessellations. After finishing a three-dimensional geometrical Voronoi algorithm Van de Weygaert & Icke (1989) found that the Voronoi tessellations also possess some interesting clustering properties. This was confirmed in a Monte-Carlo study by Yoshioka & Ikeuchi (1989). Since then, in particular the observation by Broadhurst *et al.* (1990) of a periodic redshift distribution in a deep, small solid angle, redshift survey (a "pencil beam survey") has caused an increased interest in the use of Voronoi tessellations as a useful description of the clustering of galaxies on large scales (Coles 1990; Van de Weygaert 1991a,b; Ikeuchi & Turner 1991; SubbaRao & Szalay 1992; Williams 1992; Williams *et al.* 1992).

In Van de Weygaert (1991b, 1992) we discussed at length the construction of 3-D Voronoi tessellations from a given nucleus distribution, together with the presentation of an extensive statistical analysis of the geometrical properties of the 3-D Voronoi tessellations themselves and of 2-D and 1-D sections through them. In this paper we discuss the application of these Voronoi foams to cosmology, in particular the large scale clustering of galaxies. In applying the Voronoi tessellation to the galaxy distribution we should keep in mind that they are used as paradigms for cellular galaxy distributions, without claiming that they are a perfect match to the real world. By finding some of the systematics of clustering in cellular structures we hope to be able to better understand and interpret the clustering in the far more complex situations of both the real Universe and numerical simulations.

We will adress two aspects of clustering in Voronoi foams. After a discussion of the reasons behind the use of Voronoi tessellations as a description of the large-scale clustering of galaxies

in section 2, we will treat the clustering properties of the vertices in section 4. In particular we will focus on the two-point correlation function of the vertices and compare it with that of Abell clusters. We will show that the vertex correlation function matches very well with the one inferred from observations. Since the two-point correlation function plays an important role in our analysis we describe the used estimators in section 3. Finally, in section 5 we will treat the clustering properties of points, 'galaxies', concentrated in either the walls or edges.

2. The galaxy distribution as a Voronoi tessellation

Since the beginning of the 1980's several extensive galaxy redshift surveys have become available (e.g. Sandage & Tammann 1981; Fisher & Tully 1981; Huchra *et al.* 1983). These surveys provided evidence for the early suggestion by Einasto (1978; also see Einasto, Joêveer, & Saar 1980) of cell-like structures in the distribution of galaxies. The mapping of e.g. the Local Supercluster (Tully 1982), the Coma Supercluster (Gregory & Thompson 1978), and the enormous $140h^{-1}$ Mpc long chain of galaxies forming the Perseus Supercluster (Giovanelli, Haynes, & Chincarini 1986) showed that galaxies cluster in pancake-like and filamentary structures. The discovery (Geller & Huchra 1989) of a $60 \times 170 \times 5h^{-1}$Mpc "Great Wall" of galaxies shows how large these structures can be.

In addition, the redshift surveys also revealed the existence of voids in the distribution of galaxies (Gregory & Thompson 1978; Einasto, Joêveer, & Saar 1980; Davis *et al.* 1982; Kirshner *et al.* 1981, 1987). These voids are enormous regions, tens of megaparsecs in extent, wherein few or no galaxies are found. In particular the discovery of the Boötes void (Kirshner *et al.* 1981, 1987) established them as important features of the galaxy distribution. The emerging picture of a foamlike arrangement of galaxies concentrated in walls, filaments, and clusters surrounding voids has since been supported by the publication of the CfA redshift slices (De Lapparent, Geller & Huchra 1986, 1991; Ramella, Geller & Huchra 1992), as well as its equivalent in the southern hemisphere (Da Costa & Pellegrini 1988; Da Costa 1991). Characteristic sizes of these voids are difficult to determine because these magnitude-limited redshift surveys do not probe very deep. Up till now the size of the largest observed inhomogeneities is comparable to the depth of the surveys. In fact, the recent very deep narrow-angle redshift surveys (e.g. Broadhurst *et al.* 1990) seem to suggest the existence of underdense regions with a size in the order of $130h^{-1}$ Mpc.

Some caution should be taken in not overinterpreting these structures, since the most conspicuous ones are found near the peak of the selection function of the redshift survey. Moreover, filaments in redshift sections might also be due to the type of "velocity crowding" cusps that plague galactic (l, v)-diagrams (Burton 1976; Kaiser 1987), although this cannot explain the clear filaments that are seen projected in the sky. They are quite apparent in the sky-projected distribution of 1,000,000 galaxies in the Lick counts (Shane & Wirtanen 1967; Seldner *et al.* 1977). The deeper and more accurate APM machine counts by Maddox *et al.* (1990a,b), comprising 2,000,000 galaxies on the southern hemisphere, confirm this impression of the existence of wall-like and filamentary structures (in a sky-projected distribution one cannot really distinguish between them) as well as

voids in the galaxy distribution.

One of the most important problems in the study of these large scale structures is to understand how such a foam-like distribution of galaxies can come about. Most theories of the formation of structure on large scales are based on the gravitational instability scenario (e.g. Peebles 1980). Within this scenario the existence of highly anisotropic structures as the pancakes and filaments seen in the galaxy distribution was predicted by theoretical calculations of the collapse of high-density regions, specifically of homogeneous ellipsoids in an expanding background (Oort 1970; Zel'dovich 1970; Icke 1972, 1973; White & Silk 1979; Barrow & Silk 1981). The analytical and numerical estimates from those calculations have been confirmed, extended and refined by numerous N-body simulations of the formation of structure in the Universe (Centrella & Melott 1983; Klypin & Shandarin 1983; Melott 1983; Shapiro *et al.* 1983, Frenk *et al.* 1983; Bond *et al.* 1984; Davis *et al.* 1985; Efstathiou *et al.* 1985; White *et al.* 1987a,b; Bertschinger 1991). Within the context of gravitational instability scenarios one can understand qualitatively the existence of the foam-like distribution of galaxies by exploiting the notion that not only collapsing high-density regions but also expanding underdense regions play an essential role in the formation of structure. The larger the role of voids in gravitational instability scenarios, the more the resulting structure will resemble a foam. Of course the role of the voids depends very much on the spectrum and type of primordial fluctuations, and one expects them to play a dominating role only in scenarios based on a fluctuation spectrum having a high-frequency cutoff or considerable power at low frequencies, or in scenarios with non-Gaussian primordial fluctuations having a substantial excess of underdense regions (see e.g. Moscardini *et al.* 1991).

In addition, voids also play an essential role in some non-gravitational scenarios. Especially in the explosion scenario (Ikeuchi 1981; Ostriker & Cowie 1981) the large scale structure is formed by the expanding shells of matter propelled by explosions in the early Universe. In this model a shock wave is produced by explosive energy release from first-generation objects (Yoshioka & Ikeuchi 1988) or superconducting cosmic strings (Ostriker, Thompson, & Witten 1986), sweeping up ambient intergalactic gas to a spherical shell, which fragments into new objects like galaxies. The galaxies form on the shell, and thus the bubble-like structure of the galaxy distribution is produced.

2.1 The Bubble Theorem

It was shown by Lynden-Bell (1964) and by Lin *et al.* (1965) that a homogeneous ellipsoidal dust cloud collapses in such a way that any slight departure from sphericity is systematically magnified during the evolution of the cloud. This result was extended by Icke (1972, 1973), White & Silk (1979) and Barrow & Silk (1981) to the evolution of an overdense ellipsoid in an expanding background Universe. They found that in a pressureless, selfgravitating medium, overdense fluctuations collapse to form structures with increasingly aspherical shapes, becoming flattened and filamentary. The secular increase of perturbations explains the filamentary appearance of the distribution of galaxies (Icke 1973; Oort 1983; Giovanelli *et al.* 1986; De Lapparent *et al.* 1986), but

the approximation must break down as soon as the perturbations become nonlinear.

By a simple inversion of Lynden-Bell's (1964) argument, it can be shown that the inverse of the above holds true too. A void can be considered as a negative-density region in an average background of positive density. This seems like a useless tautology, until one realizes that a reversal of the sign of the density means that *as the void becomes bigger, its asphericities will gradually disappear* (Icke 1984). This we refer to as the "Bubble theorem". These underdense fluctuations are the progenitors of the observed voids (Einasto *et al.* 1980; Kirshner *et al.* 1981, 1987). Thus, the same arguments as above still apply, except that the sense of the final effect is reversed: because a void is effectively a region of negative density in a uniform background, the voids expand while the overdense regions collapse, and slight asphericities decrease as the voids become larger. Consequently, the density in the voids becomes smaller in the course of time. Because $|\delta\rho/\rho|$ does not exceed unity in a void, the approximation will remain good for a longer period than in the case of overdense regions, except near the outer parts of the voids, where the matter gets swept up.

The tendency of underdense regions to become more and more spherical in the course of time was first seen in the N-body simulations of a three-dimensional neutrino-dominated Universe by Centrella and Melott (1983), as well as in numerical calculations of void evolution (Fujimoto 1983; Bertschinger 1985). While the "Bubble Theorem" provides a useful insight into the qualitative behaviour of a void, it is necessary to carry out more detailed studies in order to get a better understanding of physical quantities like the size distribution of voids in different clustering scenarios and density- and velocity profiles in and around voids as a function of time and initial conditions (see e.g. Ostriker & Strassler 1989; Zeng & White 1991; Van de Weygaert & Van Kampen 1993; Blumenthal *et al.* 1992; Dubinski *et al.* 1993). Just as in the case of growing filaments, the velocity field inside the voids (not in ridges surrounding them), in the regime where the quadratic potential approximation is valid, is proportional to the distance inside them. The numerical simulations by Peebles (1982), Hoffman, Salpeter, & Wasserman (1983) and Van de Weygaert & Van Kampen (1993) confirm this. Thus, voids can be described as "superhubble bubbles". For more details on the evolution of voids, and a more extensive survey of the literature on that subject, see Van de Weygaert & Van Kampen (1993).

2.2 Expanding bubbles and tessellations

From the above we can conclude that it would be sensible to construct a model of the mass distribution in the Universe based on voids since in several gravitational instability scenarios as well as in the explosion scenario they play a dominant role. Moreover, they tend to have a simple geometrical shape, in the case of the gravitational instability scenarios by virtue of the "Bubble Theorem".

We can thus "turn the Universe inside out", and consider the evolution of the *low*-density regions, which are taken to be the dominant dynamical component of the Universe. We may then think of the large-scale structure as a close packing of spheres of different sizes, generating convex cells of different sizes out of which matter flows in a slightly super-Hubble expansion towards the

interstices of the spheres, and we can think of condensations as occupying interstitial spaces of a close packing of expanding spheres of different sizes.

Consider a collection of expansion centres, the regions which are the seeds of the present-day voids. Matter flows away from these expansion centres until it encounters similar material flowing out of an adjacent void. Making the assumption that the excess expansion is the same in all voids the matter must collect on planes that perpendicularly bisect the axes connecting the 'expansion centres'. Although without doubt this is an oversimplification, Dubinski *et al.* (1993) plausibly argued that for a range of plausible fluctuation power spectra at any given epoch the Universe is filled with voids that have a narrow size distribution around a characteristic scale. The process of matter collecting on bisecting planes between 'expansion centres' leads to a geometrical skeleton of the ultimate mass distribution that is a Voronoi tessellation generated by the 'expansion centres'. In this sense the Voronoi tessellation should be considered as the tiling of comoving space into closed, convex cells; thereby one should distinguish between the mathematical Voronoi skeleton, and the actual mass density with which the skeleton is covered. The Voronoi foam should be considered as the skeleton of the matter distribution, around which the matter will assemble during the evolution of the Universe. Each cell is bounded by the bisecting planes between its expansion centre and its neighbouring expansion centres. These planes are identified with the 'walls' in the galaxy distribution. Each plane is bounded by edges, the lines where three planes meet. The density in these edges will be larger than in the planes because matter from three voids will be larger than in the planes because matter from three voids will gather in the filaments, while the planes are at the intersection of matter streaming from two voids. These edges are the filaments in the galaxy clustering. Finally, all matter will tend to stream towards the vertices of the tessellation, the highest density regions, where matter from four neighbouring voids will meet. These vertices can be identified with the Abell clusters found in the galaxy distribution.

To illustrate how Voronoi foams result from a process of expanding spheres of matter, figure 1 shows the evolution of a field of expanding two-dimensional bubbles towards a Voronoi foam. A two-dimensional illustration of the foam formation is chosen because a three-dimensional illustration would be unnecessary complicated. Different clustering processes (e.g. gravitational instability scenarios and explosion scenarios) might lead to the same Voronoi skeleton. Here we took a prescription for the bubble expansion which illustrates how a Voronoi skeleton results from a collection of expanding voids. It is closely related to the primordial explosion scenario (Ostriker & Cowie 1981; Ikeuchi 1981), and differs from the gravitational instability scenario interpretation (Icke & Van de Weygaert 1987; Van de Weygaert & Icke 1989; Icke & Van de Weygaert 1991) based on the "Bubble Theorem". In the end however, they lead to the same "tiling" of space (although the detailed matter distribution in the network will differ). We should therefore stress that figure 1a and 1b are meant as mere illustrations, and that we would rather prefer the use of the Voronoi tessellation in the gravitational instability scenario. In the beginning we have 10 nuclei and 10000 randomly distributed "matter particles". At the same instant the 10 nuclei (the same nuclei are used in both fig. 1a and fig. 1b) explode and matter is driven outwards with a velocity $v_i, (i = 1, 10)$. In figure 1a the velocities v_i are all equal, while in figure 1b they differ from nucleus to nucleus

(they are taken from a uniform distribution centred on a mean velocity $\bar{v}$, with a width of $0.6 \times \bar{v}$). This implies that we end up with a 2-D Voronoi foam in figure 1a, while figure 1b ends up with a "weighted Voronoi tessellation". The "matter particles" start expanding away from their nucleus as soon as they are hit by a shell of swept-up matter, and they keep on moving (along the line nucleus-particle) until they hit another shell. In the case of equal expansion velocities the nucleus that sweeps up the particles is the one closest to that particle, while the particles stop moving as soon as they are closer to another nucleus than to their original nucleus. In the case of the unequal expansion velocities the particles stop moving as soon as the distance d_i to their original nucleus i divided by the expansion velocity v_i, i.e. (d_i/v_i), is equal to (d_j/v_j), with j one of the other nuclei.

The Voronoi tessellation can be considered as a good approximation of the matter distribution on large scales at late times in many scenarios. As such its use does not depend on the details of the clustering process. At the same time we should stress it cannot say anything about the pattern of clustering on small scales, within the walls and filaments, nor should it claim to be a full-fledged clustering scenario. The small-scale matter distribution and the galaxy distribution itself will depend on the initial fluctuation spectrum, and on the details of the small-scale interactions of the gravitating matter. N-body simulations are preferred for solving that problem, but even those may not suffice. It seems probable that the small scale structure in the baryonic matter is considerably influenced by dissipational processes.

The primary application of the Voronoi tessellation in a cosmological context is therefore the fact that it provides us with a neatly defined mathematical model in which we can test the clustering properties of particles distributed in cellular structures. In this way a better understanding of the outcome of statistical measures from observational catalogues or N-body simulations can be achieved. For example, one might use a uniform distribution of galaxies within each wall, as was done by Yoshioka & Ikeuchi (1989), Weinberg (1989), and Van de Weygaert (1991a). One may also resort to a more realistic distribution based on an idealized description of dynamical simulations. Such a model is the kinematical model used by Van de Weygaert & Icke (1989). This is based on the notion that when matter streams out of the voids towards the Voronoi skeleton, cell walls form when material from one void encounters that from an adjacent one. In the case of these kinematic simulations the density in the centres of the walls decreases rapidly during the evolution of the cells; later, the density in the filaments decreases too, even as the matter streams towards the nodes. Thus, the walls become porous, leading to an actual matter distribution that is much more sponge-like (cf. Gott *et al.* 1986; Weinberg *et al.* 1987; Melott *et al.* 1988) than the pure Voronoi partitioning would suggest.

The Voronoi model as applied to the gravitational instability scenario is closely related to pancake theories of galaxy formation, as studied by Zel'dovich (1970), Klypin & Shandarin (1983), and Buchert (1989). Moreover, the "adhesion" approach to clustering evolution, based on the use of Burgers's equation, produces a cellular structure of dark matter which bears some resemblance to our Voronoi tessellations (Kofman & Shandarin 1988; Gurbatov, Saichev, & Shandarin 1989; Kofman 1989; Kofman, Pogosyan, & Shandarin 1990; Weinberg & Gunn 1990a,b; for a review of

these models see Shandarin & Zel'dovich 1989).

3. Setup and analysis

In order to study some of the clustering properties of Voronoi foams we generated several samples of 3-D Voronoi tessellations, both geometrically (see section 4) as well as in a Monte-Carlo fashion (see section 5) and determined the two-point correlation function of the resulting distribution of either Voronoi vertices (section 4) or particles (section 5).

3.1 The tessellation nucleus distribution

One of the points that we adress in this study is the sensitivity of the clustering properties of Voronoi tessellations to the underlying nucleus distribution. In Van de Weygaert & Icke (1989) and Van de Weygaert (1991a) we concentrated on Voronoi tessellations generated by Poissonian distributed nuclei. However, we know from the theory of Gaussian random fields (Peacock & Heavens 1985; Bardeen, Bond, Kaiser & Szalay 1986) that the likely progenitors of voids in the gravitational instability scenario, the dips in the primordial density field, are clustered. The amount of clustering of these dips is determined by the amplitude and shape of the primordial power spectrum as well as by the scale and depth of the progenitors of the present-day voids. Following this philosophy we could have generated Voronoi expansion centres by taking a primordial density field, smoothing and clipping the field on a scale and below a threshold determined by the cosmic epoch. In fact, this approach was taken by Williams (1992). However, we prefer to take a more general approach and use a one-parameter prescription for generating clustered and anticlustered nuclei. In this way we can study systematic clustering trends as a function of one parameter, thereby getting an understanding of these trends over a far larger range of possible nucleus distributions than possible in the above approach. Moreover, in this way we avoid possibly debatable identifications of expansion centres and remain independent of power spectrum.

The nuclei distribution that we explored in this study is the same as that used in Van de Weygaert (1992; also see Van de Weygaert 1991b). It consists of three classes, (1) correlated distributions, (2) a Poisson (uncorrelated) distribution and (3) anticorrelated distributions. The correlated distributions are called Class C distributions, the Poisson distribution the Class P distribution, and the anticorrelated distribution the Class A distributions.

Since there is an infinity of possible prescriptions for both correlated and anticorrelated distributions, we have to make a specific choice. For both the correlated and anticorrelated distributed nuclei we took prescriptions that conform to the ones used in the literature of stochastic geometry. In all cases 1000 nuclei were distributed in the simulation box of size $L \times L \times L$. In the case of the anticorrelated nuclei the distribution was parametrized by one parameter: the minimum distance δ between any of the nuclei (including the nuclei in the periodic extensions of the central box). We expresss δ in units of the mean distance $n^{-1/3}$ between the nuclei, n being the number

density of the nuclei. Four different anticorrelated distributions were studied in section 4, having anticorrelation parameters of $\delta = 0.8$, $\delta = 0.6$, $\delta = 0.4$ and $\delta = 0.2$ respectively. The $\delta = 0.8$ case corresponds to a very anticorrelated distribution, $\delta = 0.2$ to a midly anticorrelated distribution, while $\delta = 0.0$ is a Poissonian distribution. In the case of the correlated nuclei an adapted version of the Neymann-Scott process is used. This point process is characterized by three parameters N_0, N_1 and λ, and is constructed as follows. One starts with N_0 Poissonian distributed parent points, around each of these parent points N_1 points are uniformly distributed within a sphere of radius λ, whereby λ is expressed in units of the mean distance between the parent points, $n_0^{-1/3}$ (with n_0 the number density of the parent points). The class of correlated distributions in the present study has $N_0 = 200$ and $N_1 = 5$. Consequently, 1000 points are distributed within a box of size $100 \times 100 \times 100$. In section 4 we use four correlated distributions, having parameters $\lambda = 0.2$, $\lambda = 0.3$, $\lambda = 0.6$ and $\lambda = 1.0$ respectively. The $\lambda = 0.2$ corresponds to a very correlated nucleus distribution, while $\lambda = 1.0$ corresponds to a mildly correlated one.

Since it is rather difficult to get a good idea of the distribution of points in a three-dimensional illustration, in figure 2 we show the two-dimensional equivalents of an anti-correlated point process with $\delta = 0.8$, a Poissonian point process and a correlated point process with $\lambda = 0.4$. Instead of 1000 points in a box of size $L \times L \times L$, 100 points are distributed in a square of size $L \times L$. The mean distance between the points in both the 2-D and the 3-D case is therefore equal to L. In the case of the anticorrelated distribution the minimum distance between the points is also 0.8 times the mean distance between the points, as in the three-dimensional case. In the case of the correlated distribution, $N_0 = 33$ parent points are taken. Around each parent point $N_1 = 3$ points are distributed uniformly within a circle of radius of 0.4 times the mean distance between the parent points, $n_0^{-1/2} = L/5.74$. This parent point mean distance is about equal to one between 200 points in three dimensions.

3.2 The clustering measure: the two-point correlation function

To quantify the comparison between the Voronoi foam and the observations of the galaxy distribution, one has to derive the statistical properties of the clustering. Quantification of the complicated three-dimensional pattern in the large scale galaxy distribution, however, has proved to be a difficult task. A complete description of any point process demands higher order N-point correlation functions (Peebles 1980), yet it is practically impossible to measure $N \geq 4$ correlation functions from galaxy catalogues. This has led to the use of several techniques highlighting different geometrical properties. Here we will limit ourselves to the most widely used statistic, the two-point correlation function., $\xi(r)$. Being positioned on a random galaxy (cluster) in a sample of average galaxy (cluster) number density n, it describes the excess probability of finding another galaxy (or cluster) in a small volume δV at a distance $\vec{r}$,

$$\delta P = n\,[1 + \xi(r)]\,\delta V, \tag{2}$$

where the customary assumption of an isotropic point distribution has been made, so that ξ only

depends on $r = |\vec{r}|$.

In order to determine the two-point correlation function in our samples with errors as small as possible our estimation algorithm consists of two regimes, an estimator for large sampling radii and an estimator for small radii,

1. In the case of the large sampling radii one compares the counts around each point in the data sample with counts around that point in a catalogue of points distributed in a Poisson way in the same volume. In the sample volume a spherical sampling shell $(r - \frac{1}{2}\Delta r, r + \frac{1}{2}\Delta r)$ is centered on the coordinates of the i-th sample point. Then the number $N^i_{dd}(r)$ is the total number of points in the data sample encompassed by the shell. Notice that a part of the shell around i can be situated outside of the sample volume. The volume of this shell fraction cannot, in general, be determined analytically with reasonable effort. This problem is resolved by counting the number of points in the Poissonian sample encompassed by the same shell around the point i, denoted by the number $N^i_{dp}(r)$. This number $N^i_{dp}(r)$ can be considered as a Monte Carlo estimate of the fraction of the shell fraction inside the sample volume. Summed over i, one obtains $N_{dd}(r)$ and $N_{dp}(r)$. Then the correlation function is

$$\xi(r) = \frac{N_{dd}(r)}{N_{dp}(r)}\frac{n_p}{\bar{n}} - 1, \tag{3}$$

in which $\bar{n}$ is the number density of sample points, and n_p is the number density of Poisson points. By using this method one can neatly correct for the edge effects without losing too much information.

2. Because $N_{dp}(r)$ becomes very small at small radii (the number of Poisson points inside a shell is proportional to r^2), the $\sqrt{N}$ fluctuations in N_{dp} get too large, causing huge errors in the estimated ξ. Therefore, another estimator is used once the $\sqrt{N}$ fluctuations exceed a certain limit (10% in our implementation). The estimator used in this case relates directly to the definition of $\xi(r)$ in equation (1):

$$\xi(r) = \frac{N_{dd}(r)}{\bar{n}\sum_{i=1}^{M}\delta V_i} - 1, \tag{4}$$

where δV_i is the volume of the spherical shell with inner radius $r - \frac{1}{2}\Delta r$, and outer radius $r + \frac{1}{2}\Delta r$ centered on the i-th sample point. The number $N_{dd}(r)$ is the total number of pairs in the data sample determined by counting around each point i the number of data points in the shell $(r - \frac{1}{2}\Delta r, r + \frac{1}{2}\Delta r)$ if this shell is completely situated within the sample volume. In the case of a simple sample volume like a box this means that the point i should be at least a distance $r + \frac{1}{2}\Delta r$ from the edge of the catalog volume. If the shell lies partially outside the sample volume the corresponding pairs are discarded from the counts, because the analytical evaluation of the (partial) shell volume δV_i would take too much effort. Consequently, the count is restricted to M shell volumes. Note that a pair (i, j) will be counted twice if both the shells around i and j lie totally within the sample volume, only once if only the shell around i

or the shell around j is situated within the sample boundary, and not at all if both i and j are too close to the boundary. The number $\sum_{i=1}^{M} \delta V_i$ is the sum of the shell volumes around the M points included in the count.

The transition from estimator (1) to estimator (2) is determined by weighing the fact that $N_{dp}(r)$ in estimator (1) should not become too small against the fact that M in estimator (2) should not differ too much from the total number N of points in the sample. Practically, the use of estimator (2) was limited to a radius of 0.5% of the sample box. In the case of a uniform distribution of points this means that only 3% of the pairs is excluded from N_{dd}, which won't increase the fluctuations in the counts significantly. This percentage can be somewhat higher in the case of positive correlations on that scale, although the estimate is reasonable in the case the distribution of the data points is more or less uniform on larger scales.

4. Vertex clustering

Rich galaxy clusters are prominent features on sky survey plates. The Abell (1958) catalogue of rich clusters contains a total of 2712 clusters, identified from the Palomar Sky Survey plates by a well-defined set of selection criteria. Of these rich clusters, 1682 constitute Abell's complete statistical sample, they are distributed over 4.26 steradians of the sky. Redshifts for all clusters in Abell's statistical nearby sample of distance class $D \leq 4$ ($z \lesssim 0.1$) were measured by Hoessel, Gunn & Thuan (1980). This complete redshift sample includes 104 clusters that are of richness class $R \geq 1$ and are located at high Galactic latitude (as specified in Abell's table 1 plus the requirement of $|b| \geq 30°$). This corresponds to a mean neighbour separation of

$$\bar{d} \simeq 55 \pm 5h^{-1}\,\mathrm{Mpc}, \tag{5}$$

where the uncertainty is estimated from the Poisson errors in a sample of 104 clusters.

From this statistical sample of 104 Abell clusters Bahcall & Soneira (1983) determined the two-point spatial correlation function of clusters, $\xi_{cc}(r)$. As confirmed by several other studies (Hauser & Peebles 1973; Klypin & Kopylov 1983; Postman, Geller & Huchra 1986) the cluster-cluster two-point correlation function is well fitted by a power law over the range $7h^{-1}\,\mathrm{Mpc} \leq r \leq 100h^{-1}\,\mathrm{Mpc}$,

$$\begin{gathered} \xi_{cc}(r) = (r_0/r)^{\gamma}, \\ r_0 = 25 \pm 7h^{-1}\,\mathrm{Mpc}, \qquad \gamma = 1.8 \pm 0.3. \end{gathered} \tag{6}$$

The $\pm 7h^{-1}$ Mpc is an approximate 1σ error bar on r_0, based on the bootstrap analysis of Ling, Frenk and Barrow (1986). The error of ± 0.3 on γ was estimated by Weinberg, Ostriker & Dekel (1989) on the basis of various published studies. Beyond $100h^{-1} - 150h^{-1}$ Mpc no statistically significant correlations are observed. Thus, the rich cluster correlation function has the same shape as that of the galaxy correlation function. However, since the correlation length of the galaxy-

galaxy correlation function is only $r_0 = 5.4 \pm 0.3h^{-1}$ Mpc the clusters seem to be substantially more clustered than galaxies at the same scale.

The strong cluster correlations appear to contradict the typical cosmogenic scenarios in which clusters form from Gaussian primordial density fluctuations. In particular, the "standard" biased cold dark matter scenario (CDM), when normalized to fit the observed clustering of galaxies, cannot reproduce the high amplitude of the cluster correlation function. On the other hand, the observed increase of correlation with cluster richness (Bahcall & Soneira 1983; also see Batuski & Burns 1985; Shectman 1985; Postman *et al.* 1986; Kopylov *et al.* 1987) is explained quite naturally in these models where richer clusters correspond to higher primordial peaks (Kaiser 1984). That model has difficulty, however, in explaining the positive cluster correlations observed at large separations. Because according to this view $\xi_{cc}(r) \propto \xi(r)$ (Kaiser 1984) it predicts that ξ_{cc} should become negative beyond $r \approx 20(\Omega h^2)^{-1}$ Mpc, which is not what we observe.

It is well-known, however, that the Abell catalogue is plagued by incompleteness and projection and selection effects. This may render the above clustering results rather unreliable. For example, Soltan (1988) and Sutherland (1988) found evidence for strong anisotropies in the cluster-cluster correlation function looked at in redshift space. When corrected for projection effects the correlation amplitude is reduced to $r_0 = 14h^{-1}$ Mpc. Determination of the cluster-cluster correlation function from automatically selected cluster samples from the APM Galaxy Catalogue (Dalton *et al.* 1992) and the Edinburgh/Durham Southern Galaxy Catalogue (Nichol *et al.* 1992) yield correlation lengths of $r_0 = 14 \pm 4h^{-1}$ Mpc and $r_0 = 16.4 \pm 4.0h^{-1}$ Mpc respectively. On the other hand, the correlation function of X-ray-selected clusters (Lahav *et al.* 1989) as well as of cD clusters (West & Van den Bergh 1991) seems to support a higher value of $r_0 \simeq 21 - 22h^{-1}$ Mpc.

4.1 The Voronoi vertex-vertex correlation function

In the geometrical model represented by the Voronoi foam we identify the vertices of the tessellation with the Abell clusters in the galaxy distribution. When we test whether the vertex distribution bears any resemblance to reality, we can use the fact that *the Voronoi node distribution is a topological invariant* in co-moving coordinates, and does not depend on the way in which the walls, filaments, and nodes are populated with galaxies. Consequently, the statistics of the nodes should provide a robust measure of the Voronoi properties.

To give an impression of the distribution of our "Voronoi clusters" we have plotted in figure 3 some 1700 Voronoi vertices projected on the sky, within an area of 4.13 steradian. The corresponding Voronoi tessellation is generated by Poissonian distributed nuclei. This should be compared with the projected distribution of 1682 Abell clusters, constituting a complete statistical sample on the Northern Hemisphere (see Bahcall 1988). Although the eye is not the most objective statistical tool, the general impression is that the Voronoi vertex catalog resembles the Abell catalog quite well.

In order to be able to compare these theoretical models and observations we must specify a scaling parameter to normalize the distances in our Voronoi tessellations. We choose this parameter

to be the mean distance between the vertices, λ_V, which is put equal to the mean neighbour separation $\bar{n}^{-1/3}$ between clusters (with $\bar{n}$ being the mean number density of clusters). For $R \geq 1$ clusters this is approximately $55h^{-1}$ Mpc.

The two-point correlation function of Voronoi vertices has been determined for 9 different classes of Voronoi tessellations (see section 3.1 for the prescription of the corresponding nuclei distributions). Four different anticorrelated distributions are studied (class A), a Poissonian nucleus distribution (class P) and four different correlated distributions (class C). Of each of the 9 nucleus distributions four different realizations of 1000 nuclei were generated and the corresponding tessellations calculated geometrically (Van de Weygaert 1991b, 1992). On the basis of the four different realiztions error estimates of the two-point correlation parameters can be given. Note that this means that each correlation function is calculated on the basis of some 6700 to 6800 points, the average number of vertices per 1000 Voronoi cells (Van de Weygaert 1991b, 1992). The uncertainties in the calculated vertex-vertex correlation function due to Monte Carlo scatter is therefore rather small.

Figure 4 shows log-log plots of the resulting correlation functions for an anticorrelated nucleus distribution (case A), a Poissonian nucleus distribution (case P) and a correlated nucleus distribution (case C). The black squares are the values of the correlation function estimated from the resulting vertex distributions. The first striking observation is that the vertex-vertex correlation function appears to be a power-law over a considerable range of the distance r, something which is not at all obvious a priori. Near $r/\lambda_V \approx 0.5$ the correlation function starts to bend away from the power-law towards zero. The vertex distribution therefore appears to be homogeneous on scales larger than the mean size of a cell. Note that the correlation function in case A bends away earlier from the power-law than the correlation function in case P. In the correlated case it is precisely the reverse, its difference with a power-law around $r/\lambda_V \approx 0.5$ is only marginal. This trend is due to the fact that the range of cell sizes is considerably larger as the nuclei get more correlated (Van de Weygaert 1991b, 1993). This automatically induces correlations between vertices over a larger range of scales.

The dashed lines in the plots are power-law fits to the correlation function over the range where the power-law holds. The fits are obviously quite good. The solid lines are the power-law fits to the observed correlation function over the range $7h^{-1}$ Mpc to $100h^{-1}$ Mpc (see eqn. 6). Hereby we have used $\lambda_V = 55h^{-1}$ Mpc for the Abell clusters. All three solid lines have a slope of $\gamma = 1.8$, the thick solid line is the one corresponding to $r_0 = 25h^{-1}$ Mpc, while the lower and upper one reflect the error estimate on r_0, $7h^{-1}$ Mpc. From this we see that the two-point correlation function of the Voronoi vertices is not only a power-law over a considerable range in separtion, but that it is also in good accordance with the cluster-cluster correlation function as determined by Bahcall & Soneira (1983), both in slope and amplitude. The power-law behaviour of the Voronoi vertex-vertex correlation function was independently confirmed by Yoshioka & Ikeuchi (1989) on the basis of Monte Carlo simulations.

It is surprising that a conceptually simple geometrical model as the Voronoi foam is capable of

reproducing both slope and amplitude of the cluster-cluster two-point correlation function without making additional assumptions. This is even more striking when we realize how difficult this is for most of the popular models of large scale structure formation, in particular for the standard CDM scenario (e.g. White *et al.* 1987a,b).

Table 1 summarizes the results of the study of the systematic aspects of the Voronoi vertex-vertex correlation function of each of the 9 different nuclei distributions described above. By fitting the calculated correlation functions over the range over which they behave as power laws the slope γ and correlation length r_0 were determined. In addition, since at a certain distance the correlation functions appear to bend away from a pure power-law toward zero, estimates of the distance r_a where $\xi(r_a) = 0$ are determined. Both r_0 and r_a are specified in three different units. The first system is in units of λ_C, the mean distance between the tessellation generating nuclei. The second system is in units of the mean distance λ_V between the vertices of the tessellation. Finally, we express both r_0 and r_a in h^{-1} Mpc by putting $\lambda_V = 55h^{-1}$ Mpc, the mean distance between Abell $R \geq 1$ clusters. Several interesting observations can be made from table 1,

1. The most important observation is that both the slope γ and r_0 vary relatively little from a very anticorrelated (A 0.80) to a very correlated (C 0.20) nucleus distribution. The general conclusion is therefore that *the distribution of clusters depends only weakly on the initial conditions, and that it is determined mainly by the geometrical properties of the galaxy distribution*, i.e. their cell-like or sponge-like arrangement. Because this conclusion is purely based on the geometry of the structures which have formed, instead of their dynamics, we consider this as the key result in the study of Voronoi tessellations and their relation to large scale structures.

When looking at table 1 in somewhat more detail some (small) systematic changes of the vertex-vertex correlation function as a function of the underlying nucleus distribution can be discerned.

2. The slope of the correlation function becomes less steep when the nucleus distribution is more correlated, while at the same time the correlation length is increasing. Note that for the nuclei distributions (A 0.80) up to (C 0.60) the correlation length r_0 is still within the upper boundary of $32h^{-1}$ Mpc of the correlation function of Abell clusters.

3. The scale r_a at which ξ becomes zero is smaller when the nucleus distribution is more anticorrelated. In other words, when the nucleus distribution is more anticorrelated the correlation function bends away earlier from the power-law behaviour. For the very correlated nucleus distributions, (C 0.30) and (C 0.20), there was no sign of departure from power-law behaviour, so that r_a could not be estimated.

4. In the cases the amplitude and slope of the Voronoi vertex correlation function compare very well with the observational one, the last column of the lower panel of table 1 shows that the scale r_a is too small compared to the cited range of positive correlations in the Abell catalogue. Postman *et al.*, claim that the power law extends up to $80 - 90h^{-1}$ Mpc. A possible solution to this problem might be that the Voronoi model and the Abell classification do not attach equal weights to vertices and to clusters. Whereas in the Voronoi foam each vertex is treated similarly, in the Abell catalog only outstanding mass concentrations above some threshold are

counted. If one would e.g. argue that two vertices that are close together should effectively be considered as one cluster, the amplitude of the correlation function might decrease. In this way the amplitudes of the vertex correlation functions in the case of correlated nuclei distributions might be brought into agreement with the observational one while retaining the large extent of the power-law behaviour.

Geometrically, our models bears some resemblance to that of Weinberg, Ostriker & Dekel (1989). They based themselves on the explosion scenario of Ikeuchi (1981) and Ostriker & Cowie (1981). Using the results of the N-body simulations by Saarinen, Dekel & Carr (1987), they studied the clustering of interacting shells. In their model the clusters appear at the vertices where three shells intersect. The shells are distributed randomly throughout the volume. By investigating the model as a function of three free parameters, they try to obtain a fit to the observations. Interestingly, they also find that the vertex-vertex correlation function is a power law. However, the most succesfull choice of parameters yields the right slope but an amplitude which is too high. With these same parameters they also succeed to get a supercluster multiplicity function roughly consistent with the data. A similar model was proposed by Bahcall, Henriksen & Smith (1989) on the basis of observational considerations.

5. Clustering in walls and filaments

We know that both observations and several models of structure formation indicate that galaxies tend to cluster in a cellular network consisting of walls, filaments and nodes. However, as yet not much is known about the systematic properties of clustering in such a network. Such knowledge is very welcome in order to interpret the clustering properties of the real galaxy distribution as well as those resulting from N-body simulations. The issue we adress here specifically is to know the consequences of clustering in either filaments or walls on the two-point correlation function.

5.1 The Monte Carlo simulations

While the clustering of nodes, studied in the last section, is completeley independent of the specified distribution of galaxies, this is not true in the case of walls and filaments. In this case we need to provide a to a certain extent arbitrary prescription for the clustering within the walls and filaments. This arbitrariness implies that the applicability of the results is limited, and merely provide us with indications for interesting systematic trends. The studied particle distributions consist of particles residing within the walls or within the filaments of a Voronoi tessellation, or combinations of these two. The particle, or "galaxy", samples consist of 25,000 particles, initially randomly distributed within the simulation box. In this box with periodic boundary conditions we place 100 nuclei. Subsequently the particles are moved towards their position in a a wall or filament of the Voronoi tessellation defined by the nuclei.

In the case of the wall distribution we proceed as follows. For each of the 25000 particles we first determine the closest nucleus, the "parent nucleus". By definition the particle is situated within the Voronoi cell of that nucleus. Subsequently the particle is moved from its initial position by radial projection, along the line connecting the particle and the parent nucleus. The particle is projected onto the Voronoi wall that is first crossed by this line. This is accomplished by determining for each nucleus the crossing point of the line and the bisecting plane of the parent nucleus and the nucleus under consideration. The crossing point with the shortest distance to the initial position of the particle is the intended new position of the particle in the wall. In this way all the particles in the pyramid spanned by a particular nucleus and any of its Voronoi walls are projected onto the surface of that Voronoi wall. Consequently, the total number of particles in a Voronoi wall is proportional to the total surface area of the wall and the perpendicular distance of the nucleus to the wall. Because of the radial projection the surface number density of the walls will be uniform. The value of the surface density will differ from Voronoi wall to Voronoi wall since it is linearly proportional to the perpendicular distance of the nucleus to the Voronoi wall. Note that there is some arbitrariness in this prescription. Another possibility could have been a particle distribution wherein all Voronoi walls have the same surface density. However, the used prescription takes into account the expected variation of wall surface densities. Denser walls are expected to correspond to larger voids. The resulting distribution of particles is illustrated in figure 5a. It shows 8 consecutive slices along the Z-axis of the box, each slice having a width of 1/8th of the box width.

The filament distribution is generated in the same fashion as the wall distribution. All 25000 particles are moved to one of the edges of the Voronoi foam. First the particles are positioned in the walls according to the above description. Subsequently, the particles are moved within the wall along the line connecting their wall position and the point halfway in between the two nuclei defining the wall. Each particle ends up at the point where one of the edges of the wall intersects with this line. This is accomplished by determining for each nucleus, except of the two nuclei that define the Voronoi wall, the crossing point of this line with the bisecting plane between the "parent nucleus" and the nucleus under consideration. The crossing point with the smallest distance to the wall position of the particle is the point where the particle ends up in a filament. Effectively this procedure is a radial projection of the uniform particle distribution within the wall onto the edges surrounding the wall. The resulting particle distribution is uniform along any of the edges, although the density along each of the edges will vary from edge to edge. The resulting particle distribution is illustrated in figure 5b in the same way as that in figure 5a. Note that the filaments are infinitely thin lines.

The above prescriptions lead to walls and filaments of zero thickness. This of course bears no resemblance to the real galaxy distribution. Each particle is therefore given a random scatter around its final destination. Wall particles are first moved towards their position in the wall. Subsequently they are displaced perpendicular to the wall by a distance that is a Gaussian random variate. The standard deviation of the corresponding Gaussian distribution is the specified width of the wall. In the case of the filament particles we proceed in a similar fashion. After having

moved the particle towards its filament position it is displaced perpendicular to the edge. The displacement is isotropic around that position within the plane perpendicular to the edge, while its radial component is a Gaussian variate. As in the case of the wall the standard deviation of the corresponding distribution is the specified width of the filament. Note that the consequence of this rather arbitrary scatter recipe is that correlations on a scale lower than the width of the walls or filaments will be destroyed.

In addition to the above pure wall or filament particle distributions we also adress mixtures of these. The prescription for this is simple, and only involves the extra specification of the fraction of the 25000 particles that are located in walls and the fraction located in filaments. The wall particles are moved towards their wall position, the filament particles toward their filament position.

5.2 Clustering patterns in slices

Figure 6a-c shows three different realisations of point distributions. All three figures consist of 8 consecutive slices along the Z-axis of the simulation box. The particles are Gaussian scattered around the walls and filaments with a width of $0.025\lambda_c$, where λ_c is the average distance between nuclei. Figure 6a is a distribution of particles in filaments, figure 6c of particles in walls, while figure 6b is an intermediate case with 75% of the particles in the filaments and 25% in the walls. The resemblance to the slice redshift surveys is rather striking. In particular the intermediate case appears to be a good approximation to reality.

An interesting observation is that the slices in figure 6a clearly show a cellular pattern, although the slice boundaries cause the impression of repeatedly interrupted cell edges. This is quite remarkable since the 3-D distribution is a filamentary one, with the galaxies distributed in one-dimensional objects. It is therefore dangerous to infer from a cellular pattern in redshift slices that the three-dimensional galaxy distribution is wall-like.

Another interesting point is that some frames in figure 6 occasionally show very large voids, which in fact are compositions of the sections of several three-dimensional cells. A striking example is the void in the second slice from the left in the top row of figure 6b. Such a conglomeration of voids in a slice can be the consequence of several effects. It can be due to walls with an intrinsic low surface density or walls that are unfavourably oriented with respect tot the slice (so that their contrast is low). Another possible cause is that the filaments that form the boundary of a wall happen to lie just outside of the slice or are nearly perpendicularly oriented with respect to the slice plane. These examples show that while slice surveys contain a lot of information, one needs to take some caution when trying to infer the three-dimensional galaxy distribution from them.

5.3 Correlation analysis

Two interesting questions concerning the relationship between the two-point correlation function and a filamentary or wall-like clustering pattern are

1. whether a concentration of galaxies in filaments and walls capable of reproducing a power-law correlation function.
2. what is the clustering length r_0 as a function of the characteristic length of the clustering structures. Specifically we wish to adress the issue why the two-point galaxy-galaxy correlation function is equal to zero beyond $15h^{-1}$ Mpc while redshift surveys show that the most conspicuous structures have scales in the order of $25h^{-1} - 50h^{-1}$ Mpc. Does this indicate that something is wrong with our understanding of the large scale distribution of galaxies, or is this simply a consequence of the way galaxies cluster ?

The two-point correlation function of the filamentary or wall-like particle distributions was calculated for all 9 classes of nuclei distributions specified in table 1 (column 1). It turns out that both in the filament and the wall distributions the two-point galaxy-galaxy correlation function is even more insensitive to the nucleus distribution than the two-point correlation function of vertices. Only for very correlated and anticorrelated distributions some small systematic effects were found. This indicates that differences between clustering models on these scales are mainly caused by the small-scale clustering properties of the scenario. Consequently, we proceed solely with tessellations generated by Poissonian distributed nuclei.

Figure 7 shows, in one log-log plot, the two-point correlation function of the wall and the filament particles. The distance is expressed in units of the mean distance between nuclei, λ_c. In both cases $\xi(r)$ behaves over a considerable range like a power-law while it starts to bend towards zero around $0.4 - 0.5$ of the cell-size. In the case of the filament particles the correlation function is a near-perfect power-law that slightly bends upwards before dropping to a value of zero. The correlation function for the filaments clearly has a higher amplitude than $\xi(r)$ for the walls. This is to be expected since the filaments represent a state of stronger clustering than a distribution in walls. There is a weak indication that in the case of the walls $\xi(r)$ drops slightly below the perfect power-law values at small separations.

In conclusion we can say that purely because of geometrical reasons a galaxy distribution in a cellular network automatically leads to a power-law correlation function.

The dashed lines in figure 7 represent the power-law fits to both correlation functions. The values for the slope γ and the correlation length r_0, expressed in units of λ_c, are

$$\gamma = 1.112 \pm 0.011, \qquad r_0 = 0.144\lambda_c \pm 0.005\lambda_c \qquad \text{for walls,}$$
$$\gamma = 1.895 \pm 0.008, \qquad r_0 = 0.227\lambda_c \pm 0.005\lambda_c \qquad \text{for filaments.}$$

Note that the values for the slope γ differ considerably from the values cited by Yoshioka and Ikeuchi (1989). They quote $\gamma \sim 0.5$ and 1.5 for wall and filament particles respectively. This is quite remarkable since their Voronoi Monte Carlo simulations use practically the same prescription for the distribution of the particles in the walls and filaments.

Concerning the value of the correlation length r_0 we see that in the case of the walls $r_0/\lambda_c \sim 0.144 \sim 1/7$. This compares very well with the value of $r_0/\lambda_c = 1/8$ derived analytically by Heavens (1985) for a related clustering pattern. He assumed a distribution of galaxies in the walls of an

infinite structure of cubical cells, the walls having a constant surface density of galaxies. In that case $\xi(r)$ turns out to be a power law at small r with a slope of $\gamma = 1.0$ and a clustering length of 1/8th of the size of the cells, λ_c. Our result shows that the same result applies to a far broader, and less degenerate, class of cellular patterns. The fact that in cellular distributions the correlation lenght r_0 is so much smaller than the scale of the cells is quite a significant observation with respect to the real galaxy distribution. It explains why the galaxy correlation length of only $r_0 \sim 5h^{-1}$ Mpc is not at all in conflict with the existence of interesting structures on larger scales, as seen in e.g. the CfA redshift survey.

The same seems to hold for the filaments. Moreover, in that case the correlation function has a slope which is much closer to the one of the real galaxy distribution. From this we can conclude that the galaxy distribution is more filamentary than wall-like. As we discussed above this is not in conflict with the fact that one observes a bubble-like structure in slice surveys.

In order to test what happens if the galaxy distribution is not purely filamentary or wall-like we calculated the two-point correlation function for a whole range of mixtures. The results are shown in figure 8a. The numbers in the figure correspond to the percentage of wall and filament particles respectively. They all more or less show a power-law behaviour over a considerable range. The slope and amplitude drop in value as the percentage of wall particles increases. The power-law fits to these correlation functions are shown in figure 8b. In principle one might hope that in this way the two-point correlation function allows to determine the percentage of galaxies in filaments and walls. For completeness we just mention that a slope of 1.77 is reached for a distribution consisting of 25% wall particles and 75% filament particles. However, since the wall and filament prescriptions are rather arbitrary and artificial nothing really definitive can be concluded. The real world is far more complicated !

6. Summary and Discussion

Observations over a period of more than a decade have shown that the galaxy distribution on large scales resembles a cellular structure, with voids playing a prominent role. A lot of work has been invested already in trying to understand the formation of this kind of structures by the growth of small density fluctuations in an almost homogeneous Universe under the influence of gravity. Models based on a hierarchical buildup of structure in the Universe seem to be particulary succesfull in explaining the structure from galaxy scales up to scales of groups and clusters. A lot is known about clustering in these hierarchical scenarios, since it involves tractable mathematical problems. They seem to fail, however, to explain cell-like or foam-like arrangement of matter, consisting of voids, filaments and walls. Not yet a lot of effort has been invested into a theoretical understanding of clustering within cell structures. The main problem is that a solid mathematical background on this subject is lacking. Therefore in this paper we set out to investigate clustering properties of a statistical geometrical model that can be considered as one of the best defined paradigms for a non-regular (non-crystalline) cellular structure, the Voronoi tessellation. Although one can expect

it to have many useful applications in astrophysics, until recently this mathematical concept was not widely known. The beauty of the Voronoi tessellation is that although it is based on a simple definition it leads to a structure of great richness that as yet is still largely unexplored.

In its cosmological context the Voronoi tessellation can be considered as the skeleton of a galaxy distribution. Such a skeleton would result from an idealized model of structure formation in the Universe dominated by the expansion of underdense regions in the matter distribution. Because there are no other disturbing effects involved such an idealization provides a lot of insight into the statistical properties of a cellular distribution of galaxies. In this way a better understanding of the systematics of cellular clustering can be obtained. This is very useful when interpreting more complicated and realistic models of clustering. Since the observations teach us that such models should always contain a cellular galaxy distribution on large scales we know that this is important. The details, though, will certainly differ from the simple Voronoi model.

In this paper we adressed in some detail the clustering properties of Voronoi foams. Specifically we adressed the clustering of the vertices of a Voronoi tessellation and the clustering of particles distributed within either the walls or the edges of a Voronoi tessellation, or in mixed distributions. We concentrated mainly on the behaviour of the two-point correlation function of these distributions. Several interesting results were obtained.

The vertices of the Voronoi tessellation are identified with the galaxy clusters. For a broad set of expansion centre distributions, from very correlated to anticorrelated, the two-point correlation function of the vertices is a power-law over a considerable range of distance r. Moreover, both slope and amplitude (correlation length) of the power-laws are in accordance with the cluster-cluster correlation function of rich Abell clusters as determined by Bahcall & Soneira (1983). The variation in these parameters as a function of the expansion centre distribution is relatively small. The tentative conclusion therefore seems to be that the distribution of clusters depends only weakly on the initial conditions, and that it is determined mainly by the geometrical properties of the galaxy distribution. The small systematic variations that we found are that the slope is shallower and the correlation length larger when the expansion centre distribution is more correlated. In addition, the range of positive correlations is larger for the correlated distributions.

To study the clustering of particles within the walls and filaments of a Voronoi tessellation we need to specify a to some extent arbitrary prescription. The distributions that we studied have a uniform density in each wall and edge, with the value of the density depending on the distance of that element to the expansion centre defining the Voronoi cell. It turns out that the correlation function of both the wall particles and the filament particles is a power-law up to a distance comparable to the average cell size. The correlation function of the filaments is steeper and has a larger amplitude than that of the walls. For filaments, $\gamma = 1.9$ and $r_0 = 0.23\lambda_c$, with λ_c the average distance between the expansion centres. For walls these numbers are $\gamma = 1.1$ and $r_0 = 0.14\lambda_c$ respectively. One of the most interesting points about these numbers is that they offer a natural explanation for the fact that the galaxy-galaxy correlation function is substantially smaller than the scale of the structures displayed in the distribution of galaxies.

In conclusion we can see that the simple geometric clustering paradigm of the Voronoi tessellation offers substantial insight into the clustering of galaxies. The applications and statistical tests described in this study were limited to some specific particle distributions and to the two-point correlation function. However, at the same time we have made plausible that numerous other applications of the Voronoi tessellation can and will contribute substantially to our understanding of the intriguing patterns observed in the galaxy distribution.

Acknowledgements.

I am most indebted to Vincent Icke, this work being the product of our year-long very instructive collaboration. I am grateful to him and to Tim de Zeeuw for their assistance, comments and suggestions which were so essential in making this paper readable. I am very grateful for the encouragement, enthusiasm, advice of and discussions with Bernard Jones, which were so essential in shaping my view on Voronoi clustering. I also acknowledge useful discussions with John Peacock. Support by an International Fellowshop of the National Sciences and Engineering Research Council of Canada is acknowledged.

TABLE 1. Voronoi vertex-vertex correlation function parameters

Class	γ	r_0/λ_C	r_0/λ_V	r_0 (h^{-1} Mpc)
A 0.80	2.08 ± 0.03	0.247 ± 0.004	0.462 ± 0.009	25.4 ± 0.5
A 0.60	2.01 ± 0.03	0.276 ± 0.007	0.521 ± 0.013	28.7 ± 0.7
A 0.40	2.00 ± 0.01	0.290 ± 0.005	0.547 ± 0.009	30.1 ± 0.5
A 0.20	2.01 ± 0.02	0.291 ± 0.007	0.551 ± 0.014	30.3 ± 0.8
P 0.00	1.97 ± 0.02	0.294 ± 0.005	0.555 ± 0.010	30.5 ± 0.6
C 1.00	1.97 ± 0.01	0.304 ± 0.007	0.575 ± 0.014	31.6 ± 0.8
C 0.60	1.93 ± 0.03	0.316 ± 0.008	0.596 ± 0.015	32.8 ± 0.8
C 0.30	1.92 ± 0.01	0.326 ± 0.004	0.617 ± 0.009	33.9 ± 0.5
C 0.20	1.92 ± 0.02	0.337 ± 0.008	0.638 ± 0.015	35.1 ± 0.8

Class	r_a/λ_C	r_a/λ_V	r_a (h^{-1} Mpc)
A 0.80	0.414 ± 0.003	0.774 ± 0.005	42.6 ± 0.3
A 0.60	0.487 ± 0.012	0.918 ± 0.023	50.5 ± 1.3
A 0.40	0.514 ± 0.008	0.972 ± 0.014	53.4 ± 0.8
A 0.20	0.556 ± 0.016	1.051 ± 0.032	57.8 ± 1.8
P 0.00	0.535 ± 0.007	1.011 ± 0.014	55.6 ± 0.8
C 1.00	0.580 ± 0.012	1.096 ± 0.020	60.3 ± 1.1
C 0.60	0.652 ± 0.434	1.232 ± 0.082	67.8 ± 4.5
C 0.30	> 1.0	> 2.0	> 100.0
C 0.20	> 1.0	> 2.0	> 100.0

NOTES TO TABLE 1: The first column indicates the class of the corresponding Voronoi tessellation. The A corresponds to anticorrelated nuclei, the P to Poissonian distributed nuclei and the C to correlated nuclei. From top to bottom the correlation between the nuclei increases. For a detailed descriptions of this parameter see section 3.1. In the upper table, the second column contains the slope of the correlation function, while the third, fourth and fifth column in every first row contain the correlation length r_0 expressed in mean nucleus distance (3rd column), mean vertex distance (4th column) and in Mpc (5th column) if we put the distance between the vertices equal to the mean distance between Abell $R \geq 1$ clusters. In the lower table, the 3rd, 4th and 5th column of every second row contain the estimate of the length r_a where ξ passes through 0 for the first time, expressed in the same units as r_0 in the corresponding column in the upper table.

References

Abell, G.O., 1958, ApJS, 3, 211

Bahcall, N.A., 1988, ARA&A, 26, 631

Bahcall, N.A., & Soneira, R., 1983, ApJ, 270, 20

Bahcall, N.A., Henriksen, M.J., & Smith, T.E., 1989, ApJ, 346, L45

Bardeen, J.M., Bond, J.R., Kaiser, N., & Szalay, A.S., 1986, ApJ, 304, 15

Barrow, J.D., & Silk, J., 1981, ApJ, 250, 432

Batuski, D.J., & Burns, J.O., 1985, ApJ, 299, 5

Bertschinger, E., 1985, ApJS, 58, 1

Bertschinger, E., 1991, Computers in Physics, Mar/Apr, 164

Blumenthal, G.R., da Costa, L.N., Goldwirth, D.S., Lecar, M., & Piran, T., 1992, ApJ, 388, 234

Bond, J.R., Centrella, J., Szalay, A.S., & Wilson, J.R., 1984, MNRAS, 210, 515

Broadhurst, T.J., Ellis, R.S., Koo, D.C., & Szalay, A.S., 1990, Nature, 343, 726

Buchert, T., 1989, A&A, 223, 9

Burton, W.B., 1976, ARA&A, 14, 275

Centrella, J.M., & Melott, A.L., 1983, Nature, 305, 196

Coles, P., 1990, Nature, 346, 446

Da Costa, L.N., & Pellegrini, P.S., 1988, in Audouze, J., Pelletan, M.C., Szalay, A., eds, Proc IAU Symp. 130, Large Scale Structure in the Universe. Reidel, Dordrecht, p. 121

Da Costa, L.N., 1991, in Gerbal, D., Mamon, G.A., eds, The Distribution of Matter in the Universe. Meudon: Observatoire de Paris, in press

Dalton, G.B., Efstathiou, G., Maddox, S.J., & Sutherland, W.J., 1992, ApJ, 390, L1

Davis, M., Huchra, J., Latham, D.W., & Tonry, J., 1982, ApJ, 253, 423

Davis, M., Efstathiou, G., Frenk, C.S., & White, S.D.M., 1985, ApJ, 292, 371

De Lapparent, V., Geller, M.J., & Huchra, J.P., 1986, ApJ, 302, L1

De Lapparent, V., Geller, M.J., & Huchra, J.P., 1991, ApJ, 369, 273

Dubinski, J., da Costa, L.N., Goldwirth, D.S., Lecar, M., & Piran, T., 1993, ApJ, in press

Efstathiou, G., Davis, M., Frenk, C.S., & White, S.D.M., 1985, ApJS, 57, 241

Einasto, J., 1978, in Longair, M.S., Einasto, J., eds., Proc. IAU Symp. 79, The Large Scale Structure of the Universe. Reidel, Dordrecht, p. 52

Einasto, J., Joêveer, M., & Saar, E., 1980, MNRAS, 193, 353

Fisher, J.R., & Tully, R.B., 1981, ApJ, 47, 139

Frenk, C.S., White, S.D.M., & Davis, M., 1983, ApJ, 271, 9

Fujimoto, M., 1983, PASJ, 35, 159

Geller, M., & Huchra, J., 1989, Sci, 246, 897

Giovanelli, R., Haynes, M.P., & Chincarini, G.L., 1986, ApJ, 300, 77

Gott, J.R., Melott, A.L., & Dickinson, M., 1986, ApJ, 306, 341

Gregory, S.A., & Thompson, L.A., 1978, ApJ, 222, 784

Gurbatov, S.N., Saichev, A.I., & Shandarin, S.F., 1989, MNRAS, 236, 385

Hauser, M.G., & Peebles, P.J.E., 1973, ApJ, 185, 757

Heavens, A., 1985, MNRAS, 213, 143

Hoessel, J.G., Gunn, J.E., & Thuan, T.X., 1980, ApJ, 241, 486

Hoffman, G.L., Salpeter, E.E., & Wasserman, I., 1983, ApJ, 268, 527

Huchra, J.P., Davis, M., Latham, D., & Sandage, A.R., 1983, ApJS, 52, 89

Icke, V., 1972, Formation of Galaxies Inside Clusters, Ph.D. Thesis, Leiden University

Icke, V., 1973, A&A, 27, 1

Icke, V., & Van de Weygaert, R., 1987, A&A, 184, 16

Icke, V., & Van de Weygaert, R., 1991, QJRAS, 32, 85

Ikeuchi, S., 1981, PASJ, 33, 211

Ikeuchi, S., & Turner, E.L., 1991, MNRAS, in press

Kaiser, N., 1984, ApJ, 284, L9

Kaiser, N., 1987, MNRAS 227, 1

Kiang, T., 1966, Zeitschr. f. Astrophys., 64, 433

Kirshner, R.P., Oemler, A., Schechter, P.L., & Shectman, S.A., 1981, ApJ, 249, L57

Kirshner, R.P., Oemler, A., Schechter, P.L., & Shectman, S.A., 1987, ApJ, 314, 493

Klypin, A.A., & Kopylov, A.I., 1983, SvA, 9, 41

Klypin, A.A., & Shandarin, S.F., 1983, MNRAS, 204, 891

Kofman, L.A., 1989, in Cracow Summer School on Cosmology, August 1988, to be published by Springer

Kofman, L.A., & Shandarin, S.F., 1988, Nature, 334, 129

Kofman, L.A., Pogosyan, D., & Shandarin, S.F., 1990, MNRAS, 242, 200

Kopylov, A.I., Kuznetsov, D.Yu., Fetisova, T.S., & Shvartsman, V.F., 1987, in Proc. Semin. Large Scale Structure of the Universe, 1986, Stavropol, USSR, Spec. Astrophys. Obs., p.39

Lahav, O., Edge, A., Fabian, A.C., & Putney, A., 1989, MNRAS, 238, 881

Lin, C.C., Mestel, L., & Shu, F.H., 1965, ApJ, 142, 1431

Ling, E.N., Frenk, C.S., & Barrow, J.D., 1986, MNRAS, 223, 21P

Lynden-Bell, D., 1964, ApJ, 139, 1195

Maddox, S.J., Sutherland, W.J., Efstathiou, G., & Loveday, J., 1990a, MNRAS, 243, 692

Maddox, S.J., Efstathiou, G., & Sutherland, W.J., 1990b, MNRAS, 246, 433

Matsuda, T., & Shima, E., 1984, Prog. Theor. Phys., 71, 855

Melott, A.L., 1983, MNRAS, 205, 637

Melott, A.L., Weinberg, D.H., & Gott, J.R., 1988, ApJ, 328, 50

Møller, J., 1989, Adv. Appl. Prob., 21, 37

Moscardini, L., Matarrese, S., Lucchin, F., & Messina, A., 1991, MNRAS, 248, 424

Nichol, R.C., Collins, C.A., Guzzo, L., & Lumsden, S.L., 1992, MNRAS, 255, 21P

Oort, J.H., 1970, A&A, 7, 381

Oort, J.H., 1983, ARA&A, 21, 373

Ostriker, J.P., & Cowie, L.L., 1981, ApJ, 243, L127

Ostriker, J.P., Thompson, C., & Witten, E., 1986, Phys. Lett., B 180, 231

Ostriker, J.P., & Strassler, M., 1989, ApJ, 338, 579

Peacock, J.A., & Heavens, A.F., 1985, MNRAS, 217, 805

Peebles, P.J.E., 1980, The Large-Scale Structure of the Universe. Princeton Univ. Press
Peebles, P.J.E., 1982, ApJ, 257, 438
Postman, M., Geller, M., & Huchra, J.P., 1986, AJ 91, 1267
Ramella, M., Geller, M.J., & Huchra, J.P., 1992, ApJ, 396
Saarinen, S., Dekel, A., & Carr, B., 1987, Nature, 314, 598
Sandage, A., & Tammann, G.A., 1981, A Revised Shapley-Ames Catalog of Bright Galaxies, Carnegie Inst. Washington, Publ. 633
Seldner, M., Siebers, B., Groth, E.J., & Peebles, P.J.E., 1977, A.J., 82, 249
Shandarin, S.F., & Zel'dovich, Ya.B., 1989, Revs. Mod. Phys. 61, 185
Shane, C.D., & Wirtanen, C.A., 1967, Publ. Lick Obs., 22, Part 1
Shapiro, P.R., Struck-Marcell, C., & Melott, A.L., 1983, ApJ, 275, 413
Shectman, S., 1985, ApJS, 57, 77
Soltan, A., 1988, MNRAS, 231, 309
SubbaRao, M.U., & Szalay, A.S., 1992, ApJ, 391, 483
Sutherland, W., 1988, MNRAS, 234, 159
Thompson, C., Weinberg, D.H., & Juskiewicz, R., 1989, preprint
Tully, R.B., 1982, ApJ, 257, 389
Van de Weygaert, R., 1991a, MNRAS, 249, 159
Van de Weygaert, R., 1991b, Voids and the Geometry of Large Scale Structure, Ph.D. thesis, Leiden University
Van de Weygaert, R., 1992, A&A, preprint
Van de Weygaert, R., & Icke, V., 1989, A&A, 213, 1
Van de Weygaert, R., & Van Kampen, E., 1993, MNRAS, in press
Weinberg, D.H., 1989, Reconstructing Primordial Density Fluctuations, Ph.D. thesis, Princeton University
Weinberg, D.H., Gott, J.R., & Melott, A.L., 1987, ApJ, 321, 2
Weinberg, D.H., Ostriker, J.P., & Dekel, A., 1989, ApJ, 336, 9
Weinberg, D.H., & Gunn, J.E., 1990a, ApJ, 352, L25
Weinberg, D.H., & Gunn, J.E., 1990b, MNRAS, 247, 260
West, M.J., & Van den Bergh, S., 1991, ApJ, 373, 1
White, S.D.M., & Silk, J., 1979, ApJ, 231, 1
White, S.D.M., Frenk, C.S., Davis, M., & Efstathiou, G., 1987a, ApJ, 313, 505
White, S.D.M., Davis, M., Efstathiou, G., & Frenk, C.S., 1987b, Nature, 330, 451
Williams, B.G., 1992, Hierarchical and Cellular Structures in Cosmology, Ph.D. thesis, Univ. Edinburgh
Williams, B.G., Peacock, J.A., & Heavens, A.F., 1991, MNRAS, 252, 43
Yoshioka, S., & Ikeuchi, S., 1989, ApJ, 341, 16
Zel'dovich, Ya.B., 1970, A&A, 5, 84
Zeng, N., and White, S.D.M., 1991, ApJ, 374, 1

Figure Captions

FIGURE 1a. The formation of a Voronoi tessellation as a result of bubble expansion. The depicted model mainly serves illustration purposes and is not the picture of LSS formation we have in mind (see text). Each frame contains 10000 particles and 10 expansion centres. The nuclei are distributed randomly, as were the particles originally. Subsequently bubbles start expanding at the same rate from all 10 nuclei, sweeping up the particles. Each particle stops moving as soon as it hits another expanding bubble. The figure shows a sequence of 6 consecutive timesteps of this process. At the last timestep all particles have ended up in the edges of the Voronoi tessellation. FIGURE 1b. Same as figure 1a. The expansion centres have the same spatial distribution, but the expansion rates of the expansion centres are different. Consequently, the particles end up in a generalized Voronoi tessellation with curved edges.

FIGURE 2. Two-dimensional point distributions equivalent in clustering properties to the three-dimensional nuclei distributions described in section 3.1. Instead of 1000 points in a box of size $L \times L \times L$ here 100 points are distributed in a square of size $L \times L$ in such a way that the relative distances of the points are the same in the 3-D point process as in the 2-D point process. These pictures can therefore be considered as projections of a slice taken out of the 3-D box with a width of 1/10th of the boxsize. In this way we hope to give a better idea of the point process than with a full 3-D illustration. Left: correlated distribution, $\lambda = 0.4$; Middle: Poissonian distribution, $\delta = 0.0$; Right: anticorrelated distribution, $\delta = 0.8$.

FIGURE 3. Projected distribution of 1700 Voronoi vertices on the sky within a solid angle of 4.13 steradian. This distribution should be compared to the distribution of 1682 Abell clusters on the Northern Hemisphere within 4.26 steradian as is shown in figure 2 of Bahcall (1988).

FIGURE 4. The spatial vertex-vertex correlation function of a Voronoi foam with 1000 nuclei. The left panel corresponds to a Voronoi foam generated by anticorrelated nuclei, the central panel to a Voronoi foam generated by Poissonian distributed nuclei, and the right panel to a Voronoi foam generated by correlated nuclei. The distance is expressed in units of the mean distance between vertices, λ_V. The black dots are the results of the Monte Carlo simulations and the dashed lines are the power-law fits to these results. The solid lines correspond to the power-law fit to the observational data by Bahcall & Soneira (1983), with the outer solid lines indicating the range allowed by the uncertainties in the data (see eqn. 6).

FIGURE 5a. Slices through a distribution of 25000 particles in the walls of a Voronoi foam of 25 cells. The simulation box has periodic boundary conditions. The walls in the particle distribution are infinitely thin. Shown are eight consecutive slices through the box in the Z-direction, each slice having a width of $1/8th$ of the box size. The top left slice is the slice with the highest Z-value, the lower right slice the one with the lowest Z-value. FIGURE 5b. Same as figure 5a, but then for 25000 particles in the edges of a Voronoi foam. The edges are infinitely thin.

FIGURE 6. Slices through three different realizations of distributions of 25000 particles in the walls and filaments of a Voronoi foam of 25 cells. In (a) all particles are in the filaments, in figure (c) all particles are in the walls, while in figure (b) 75% of the particles is in filaments and 25% in walls. Both the walls and the filaments in the 3-D distribution have a finite width of 0.025 times the mean distance between nuclei, λ_c. As in figure 5 the simulation box has periodic boundary conditions, while the order of the slices is the same.

FIGURE 7. The two-point correlation function of particles distributed in the walls of a Voronoi foam (hexagons), and of particles distributed in the filaments of a Voronoi foam (squares). The dashed lines represent power-law fits to these functions. Distance is expressed in units of the mean nucleus distance λ_c.

FIGURE 8. The two-point correlation functions of particles that are distributed in the walls and filaments of a Voronoi foam. The functions shown are for seven different mixtures of particle distributions. The numbers in the insert denote the corresponding percentages of particles in the walls and filaments. The number before the slash gives the percentage in walls, the number behind the slash the percentage in the filaments. The left frame shows the calculated correlation function, the right frame the corresponding power-law fits. Distances are expressed in units of the average nucleus distance, λ_c.

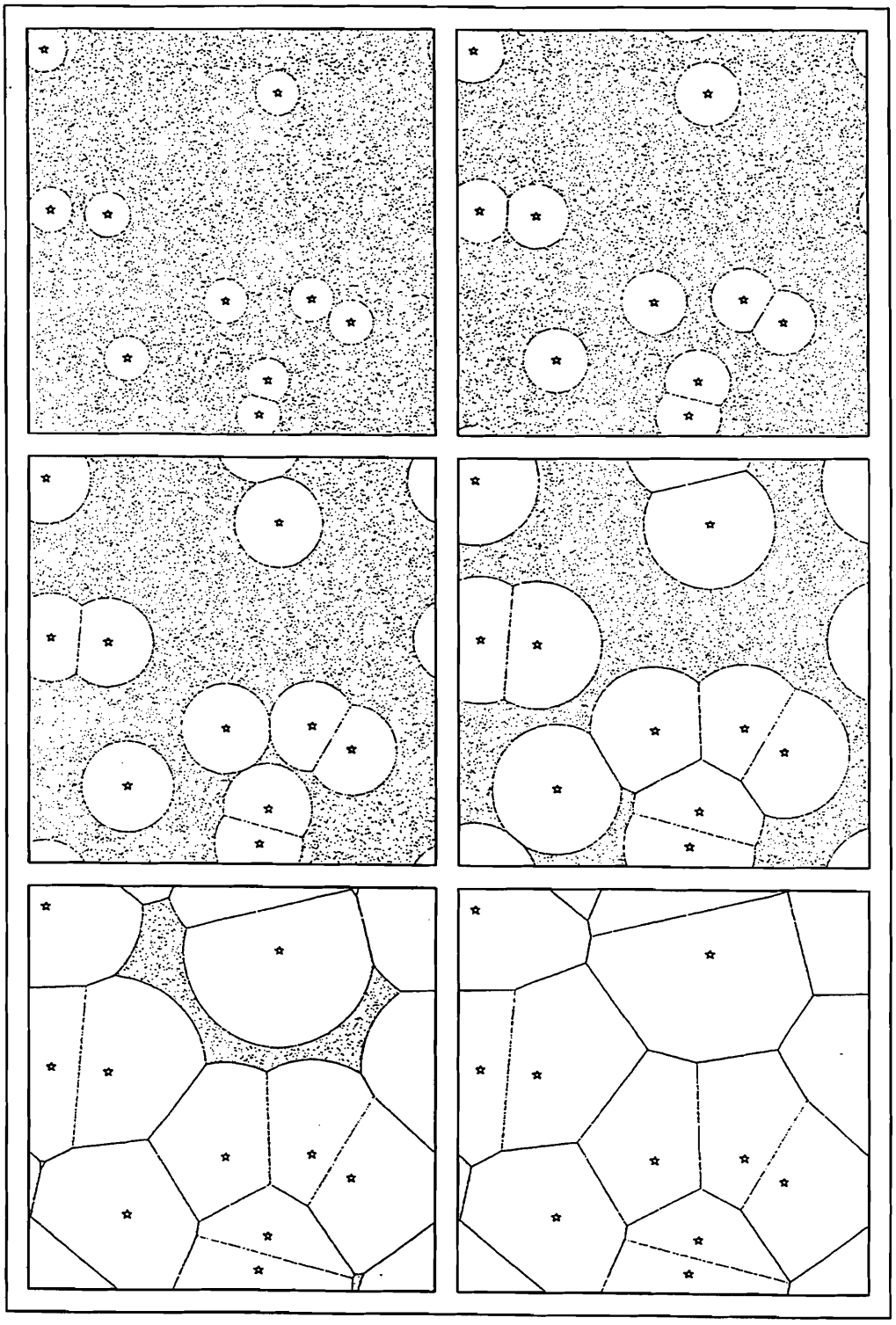

Figure 1a

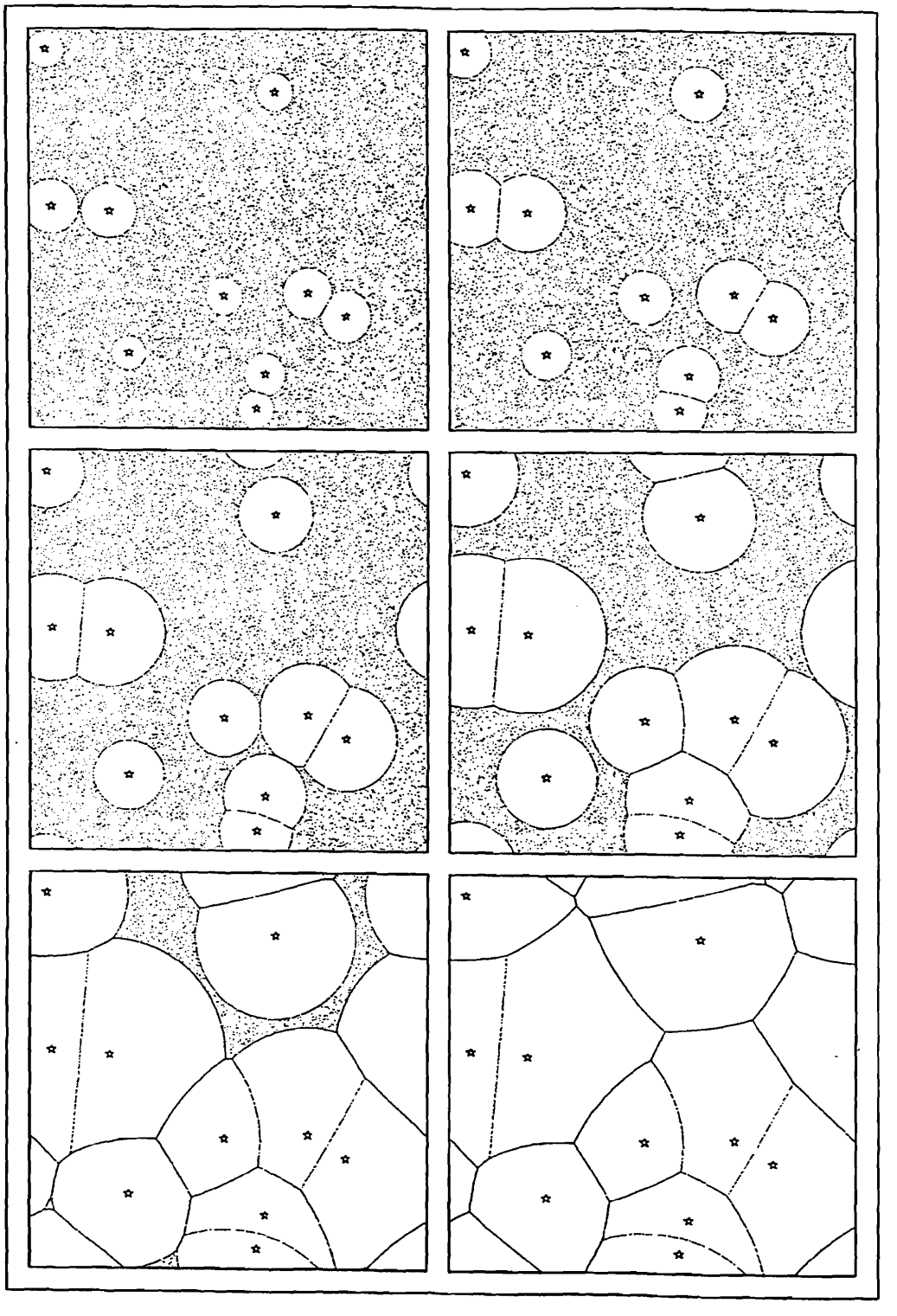

Figure 1b

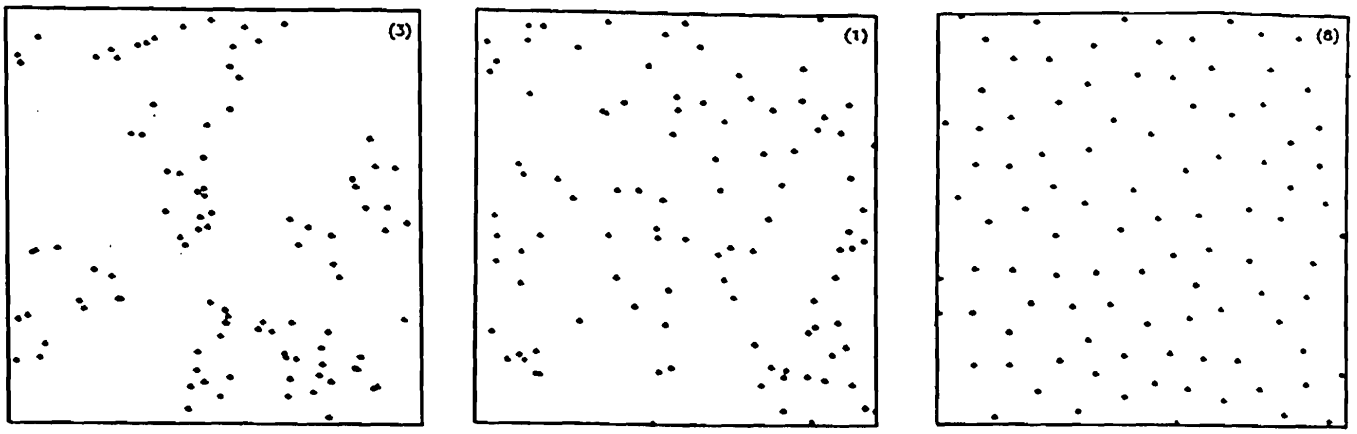

Figure 2

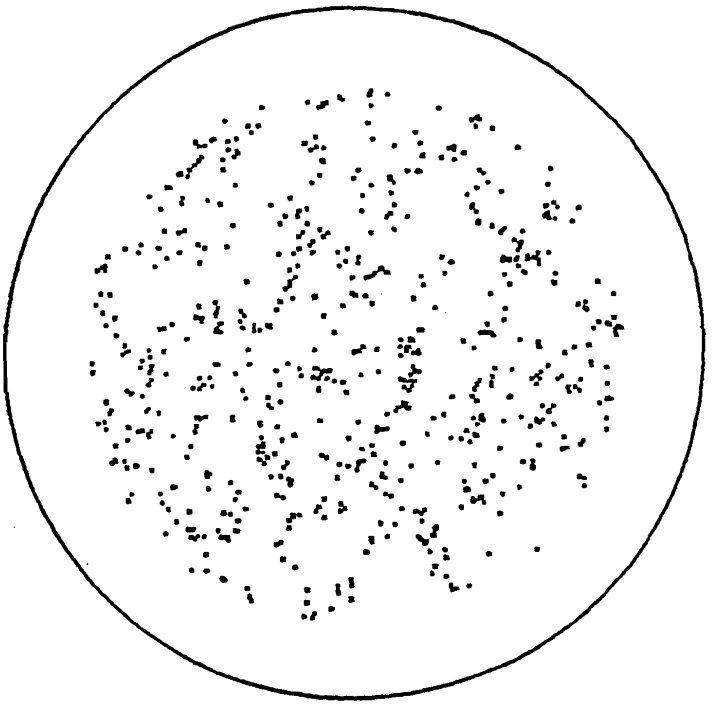

Figure 3

Figure 4

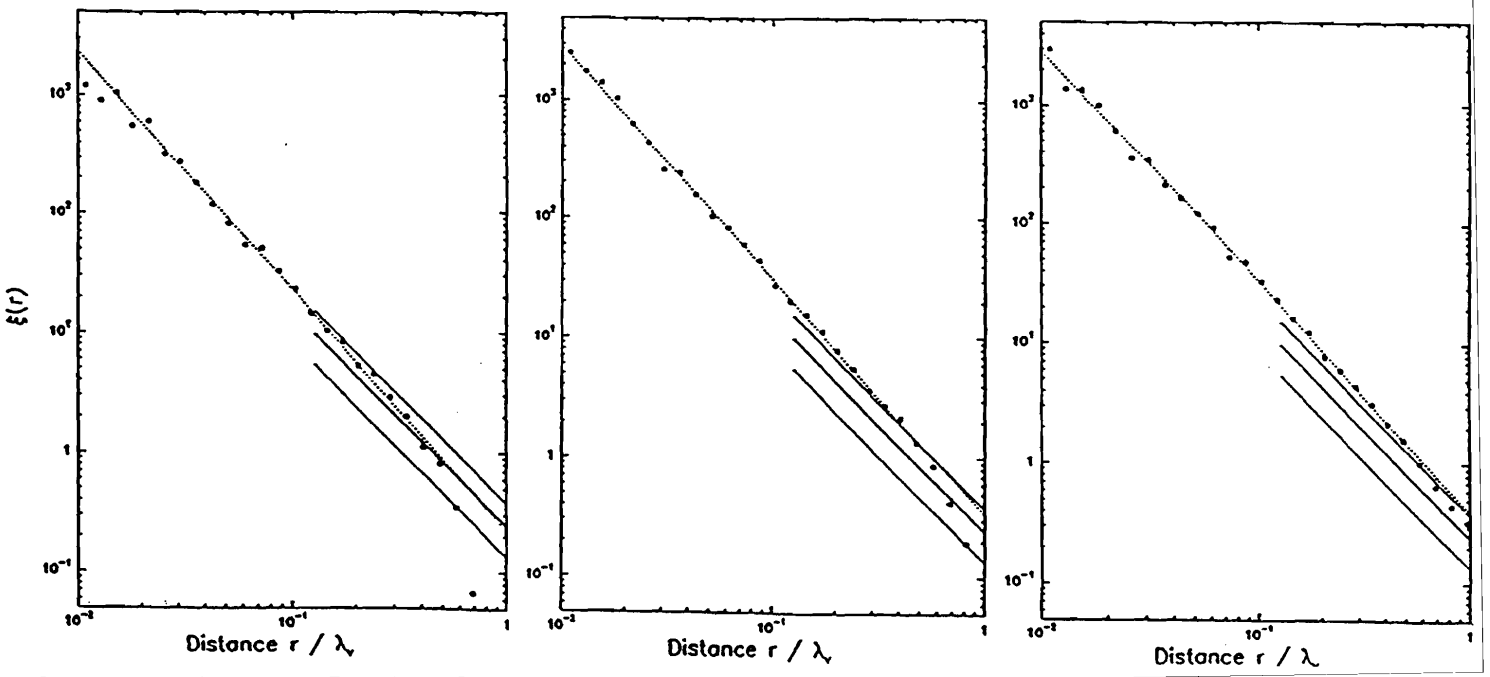

Figure 5a

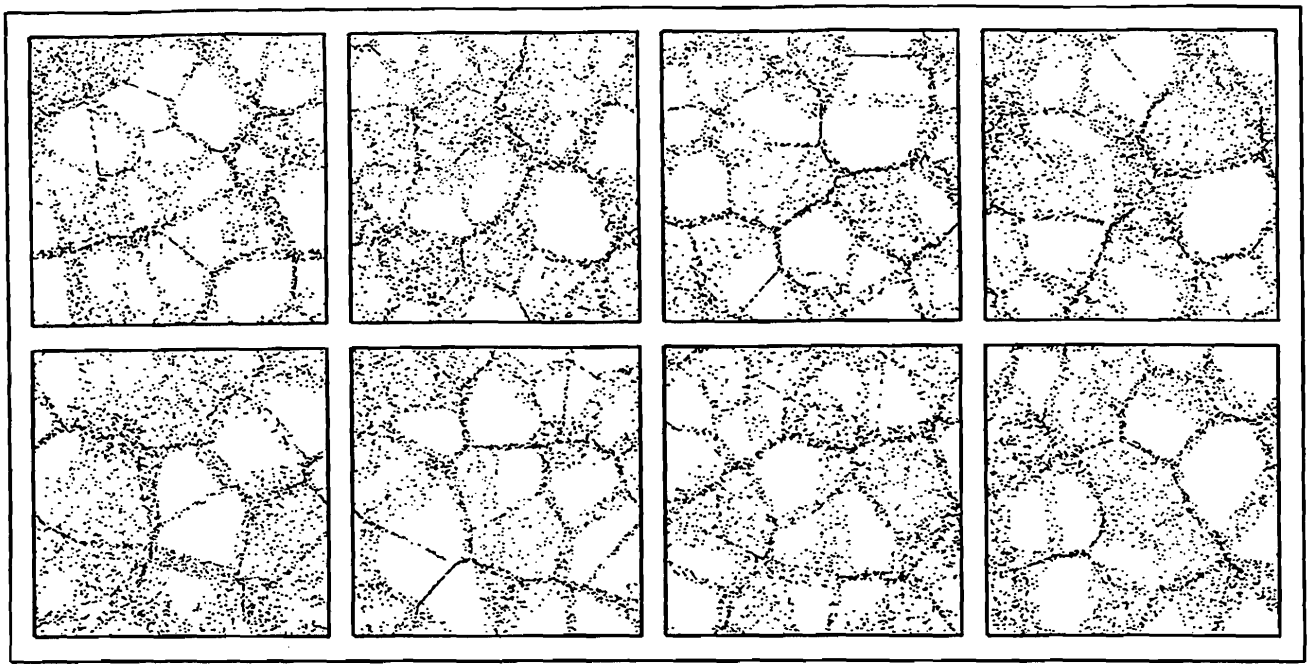

Figure 5b

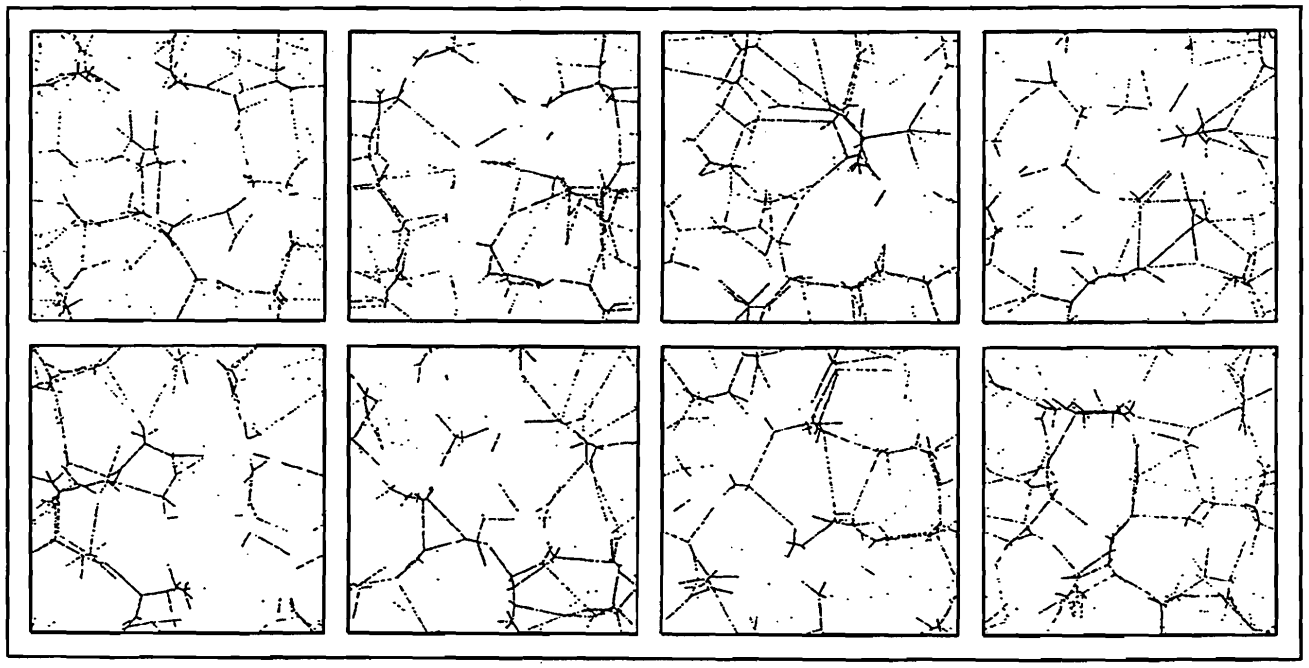

a

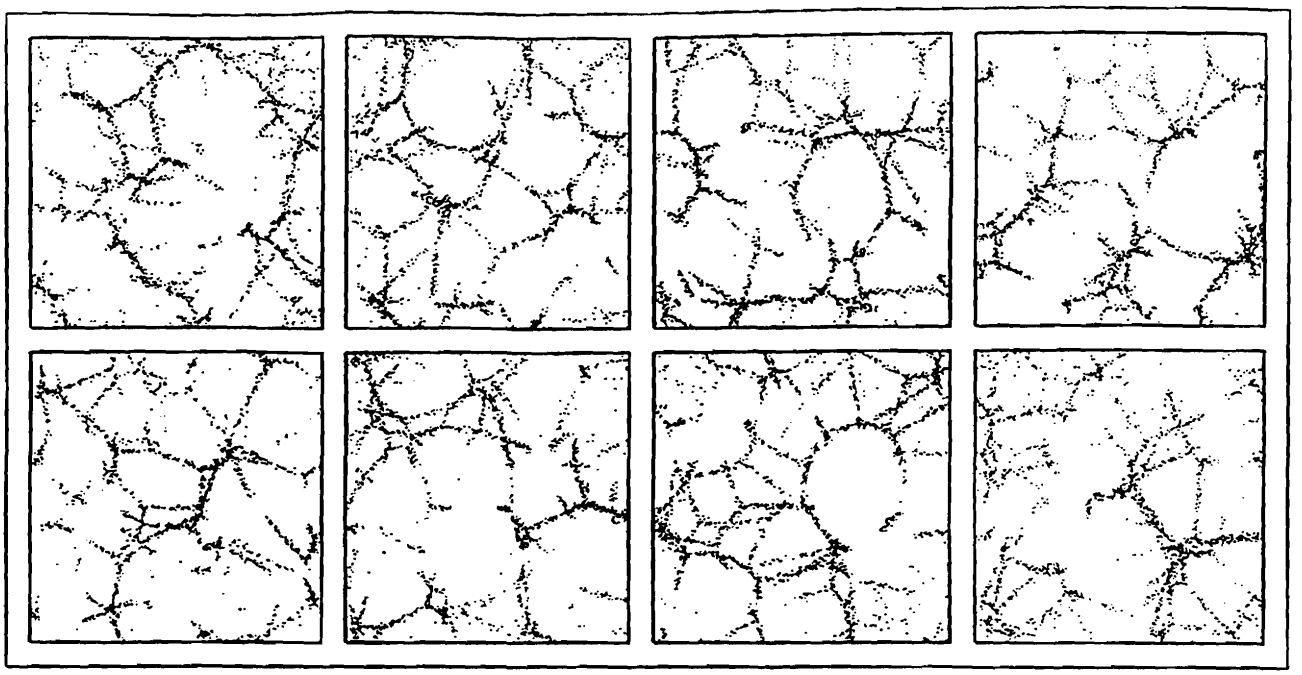

b

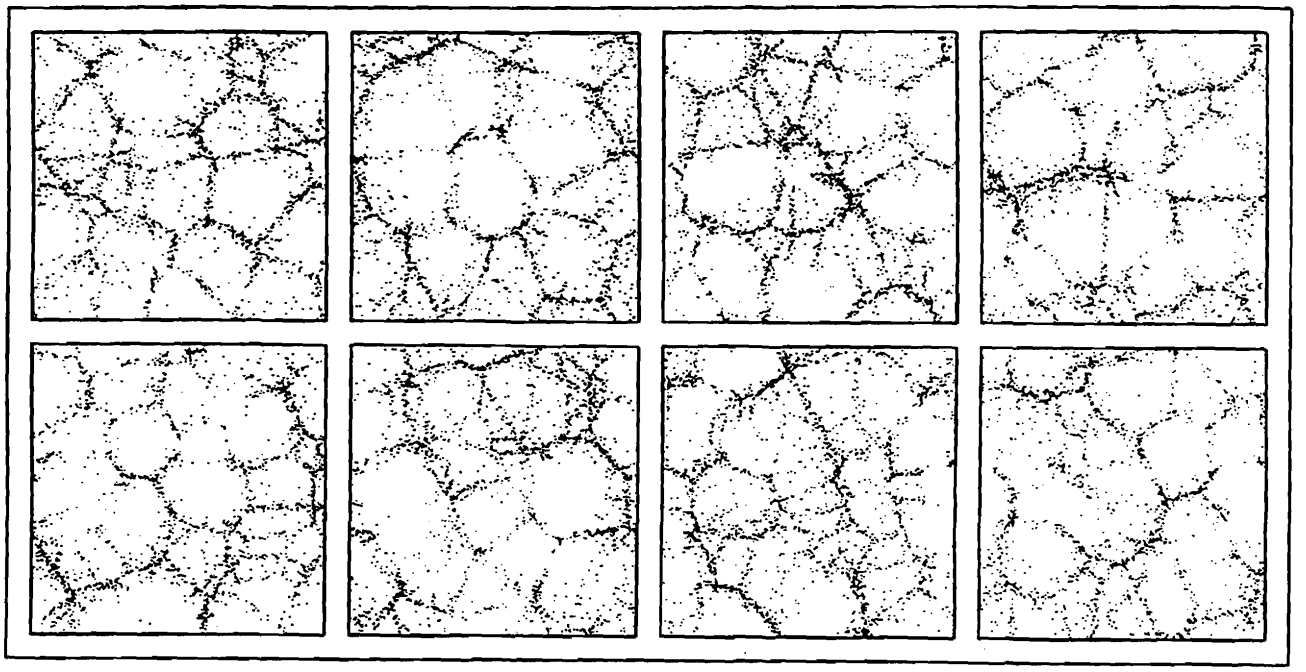

c

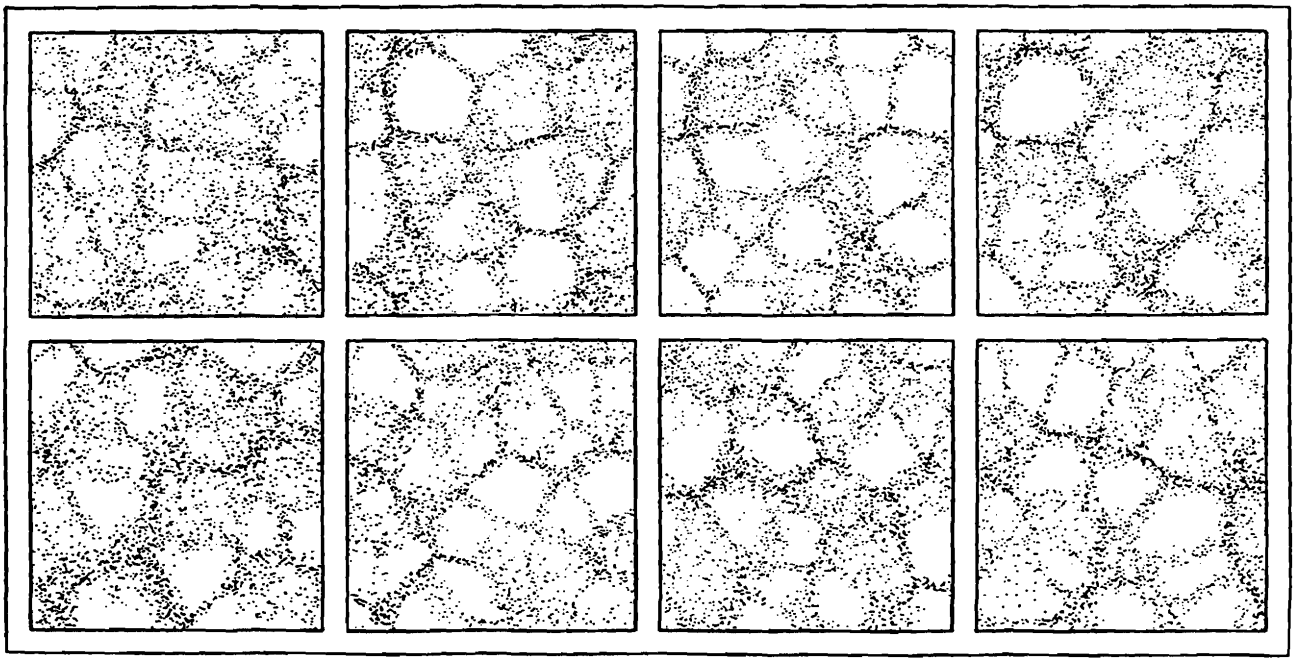

Figure 7

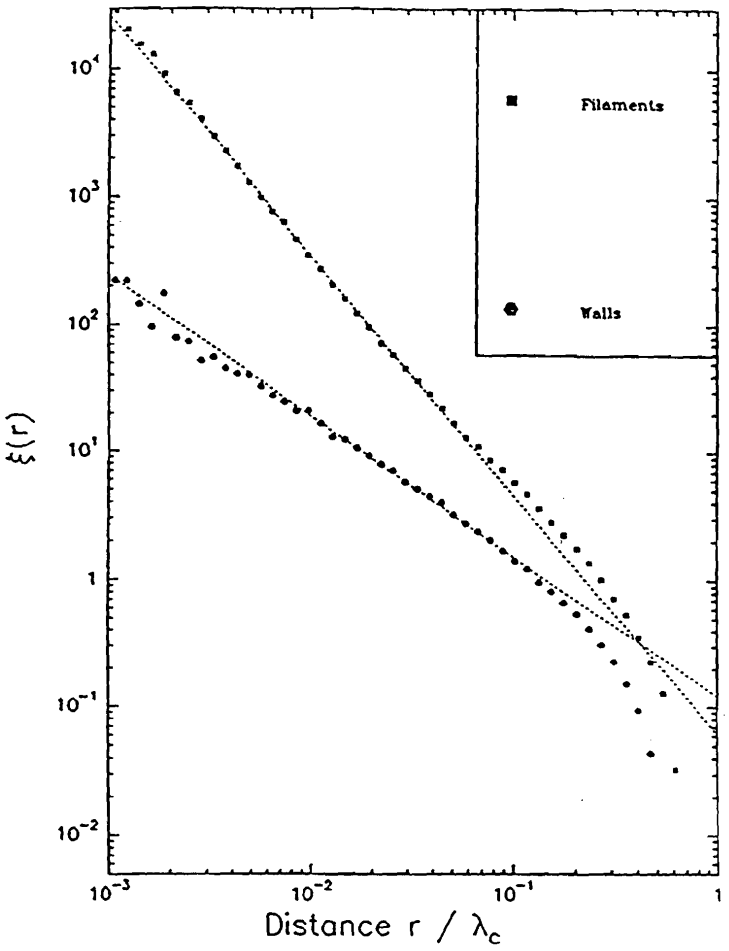

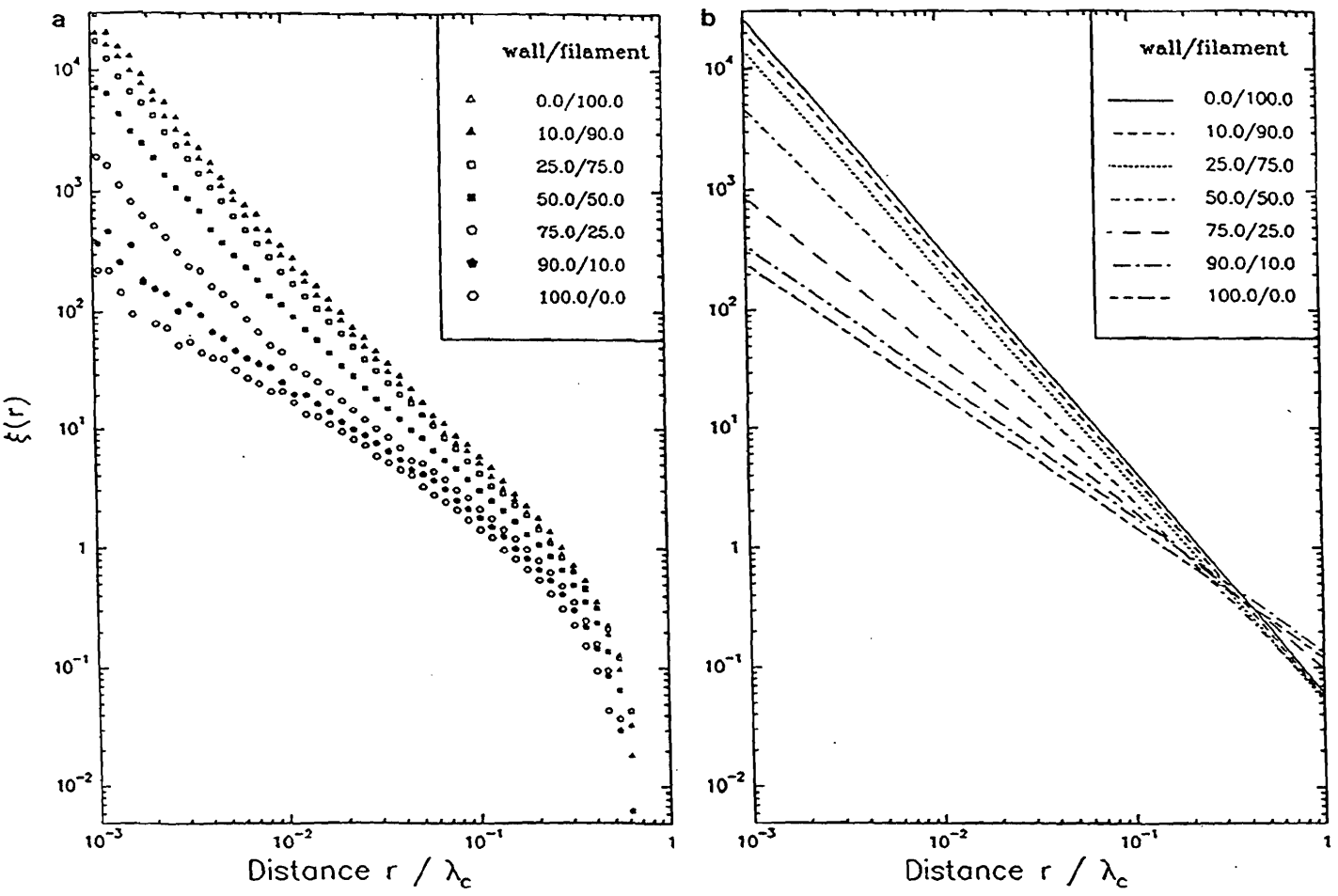

Figure 8